# A Study of Distances and the Baryon Acoustic Oscillations in Curved Spacetimes

Alan Clarke

Thesis presented for the degree of Master of Science
In the Department of Mathematics and Applied Mathematics
University of Cape Town

September 2012

Supervisor: Professor Bruce Bassett

**Abstract**

The Baryon Acoustic Oscillations offer a powerful method of measuring cosmological distances and the expansion history of the Universe. Understanding of the BAO comes from linear physics and allows for accurate predictions of the BAO scale. This will result in accurate measurements of the parameters of the Universe. Currently, most BAO measurements assume a flat cosmology; this work seeks to investigate if the assumption of flatness provides inaccuracies in the measurement process. First, the angular diameter distance and the Hubble parameter are studied in models with different curvature densities to determine how these measurements change with cosmology. Then, to investigate how the BAO signal changes with curvature, a model universe with a closed geometry is simulated. In this model universe, a galaxy catalogue is created with a strong BAO signal which is then measured via the 2-point correlation function for both the created cosmology and for a flat universe, and the results are compared. The acoustic signal is seen to shift from $151.1 \pm 1.9$ Mpc to $149.8 \pm 1.9$ Mpc, with the important result that the shift in the acoustic scale is independent of redshift.

# Contents

**Plagiarism Declaration**

I know the meaning of plagiarism and declare that all of the work in the document, save for that which is properly acknowledged, is my own.

**Acknowledgements**

Academic research has been a new and exciting challenge at this stage in my life. It would not have gone as well as it did if not for the support of many different people. First, my thanks go to my family for the constant support and unconditional love; to my parents for advice when asked (or unasked) and always believing that I am more capable than I could dream, and my brothers for always sharing a joke and humouring me with my stranger ideas and fancies.

I am lucky to have made many new friends in the past three years. Their quirks and character have made my days in Cape Town that little bit more special.

Thanks go to my office mates; Michelle, Patrice, Eli, Nima, and Navin for the interesting discussions about life, the Universe and everything, and for providing assistance when I encountered particularly stubborn problems.

Thanks must go to the National Astrophysics and Space Science Program for the opportunity to study the field of science I am most passionate about, without NASSP I would not be here today. Also, my thanks go to the African Institute for Mathematical Sciences for hosting me for the duration of researching this project.

Lastly, my thanks go to my supervisor Bruce for always providing assistance and guidance throughout this project. By not telling me the answers to my problems, but instead gently pointing in a direction and leaving me to put the various parts together he gave me the greatest gift of all, the realisation that I can do more than I thought myself capable of and a trust in my own ability to solve any problem that might come my way.

Thank you.

# Chapter 1

# Standard Cosmology

## 1.1 A Brief History of Cosmology

Cosmology is the study of the origin, evolution and fate of the Universe as a whole, as well as a study of the laws that govern the Universe and bring order to it. Ultimately, cosmology seeks to answer the question "Why are we here and where are we going?" Marcus Aurelius wrote in his *Meditations* that [1]

> Someone who does not know that there is an ordered Universe does not know where he is. Someone who does not know the natural purpose of the Universe does not know who he is or what the Universe is. Someone who fails in any one of these ways could not tell the purpose of his own existence either.

Man has been looking for explanations for the Universe and the nature of reality since he could first perceive the world around him, with the first explanations given in the creation myths of various religions and cultures around the world. With the rise of Greek culture around 500 BC the explanations offered were of a more intuitive nature. The Ancient Greek philosophers sought to understand nature through observation and logic, leading to the first underpinnings of modern scientific enquiry.

Everything changed in 1543 with the publication of *De Revolutionibus Orbium Coelestium* by Nicolaus Copernicus. This combined with Galileo Galilei's observations of the solar system and stars, led to the beginning of the Scientific Revolution. The development of calculus by Sir Isaac Newton then launched a systematic investigation into the workings of the Universe, with much of classical physics being uncovered in the following centuries.

Modern physical cosmology began at the beginning of the 20th century. First, a deeper understanding of the nature of light was achieved by Albert Einstein in 1905. In an idea first proposed by Hendrik Lorentz, Einstein created Special Relativity by removing the idea of absolute time and space and instead relating time and space to the observer. He also established the speed of light as an upper bound on speed limits. Second, Einstein took Max Planck's idea of quantised particles and applied it to light to solve the photo-electric effect. These two ideas were the basis for the modern theories of physics, General Relativity and Quantum Mechanics.

In 1915 Einstein published his theory of General Relativity, arguing that gravity is not a force, as Newton proposed, but is instead an effect of the geometry of spacetime, which is caused by space being curved in the presence of mass or energy. This led to many models being proposed, the most important of which is the Friedmann-Lemaître-Robertson-Walker (FLRW) model, which is the currently accepted model for the Universe. The FLRW model argues for a homogenous, isotropic expanding or contracting universe.

Concurrent strides were also being made in observations to match the aforementioned theoretical achievements. In 1922 Edwin Hubble's observations of Cepheid variables, combined with Vesto Slipher's discovery that the observed spectrum of galaxies was red-shifted, led to the creation of Hubble's Law, the first indication that the Universe is expanding. Observations of the rotation curves of galaxies in the Coma Cluster led to the proposal of dark matter to explain the discrepancy between the greater mass observed by the rotation curves and the mass suggested by the luminosity of the galaxies.

Due to the discovery that space was expanding, it began to become clear to others that the Universe must have been much smaller in the past. This led to the proposal of the "Big Bang." Part of this theory was that there must be radiation left over from this expansion of space. The Cosmic Microwave Background Radiation was then discovered by Arno Penzias and Robert Wilson in 1965, leading to the abandonment of a steady state universe and the acceptance of a universe that began from an initial singularity.

In 1980 Alan Guth proposed inflation, the idea that very early after the Big Bang, approximately $10^{-32}$ seconds after, the Universe underwent incredibly rapid expansion in a brief period of time, around $10^{-36}$ seconds in length. This expansion results in all the regions of the Universe being in causal connection with each other, and explains why

instead of observing a highly curved, heterogenous space-time as Big Bang physics would suggest, a flat, homogenous and isotropic universe is observed instead. The last big idea to be discovered in modern cosmology is that not only is the Universe expanding, this expansion is accelerating. This has led to the proposal of dark energy, thus reviving Einstein's earlier idea of a cosmological constant, though not for the purposfullpagees he had in mind.

## 1.2 General Relativity

General Relativity (GR) is a classical theory of gravity which has the simple premise that gravity is not a force but is instead the curvature of the geometry of spacetime in the presence of matter or energy. At the heart of GR is the equivalence principle; that gravity and inertia are equivalent for a freely falling observer, as far as local physical experiments are concerned [2]. GR is written in the mathematical language of tensor calculus. The reason for this is that tensors can express physics and geometry in any coordinate system and can translate from one coordinate system to another without losing the relationships between coordinate points. The following section introduces the concepts of GR.



### 1.2.1 The Metric

In the general case of an $n$-dimensional spacetime with coordinates $x^\alpha = \{x^1, x^2, \ldots, x^n\}$, the metric tensor, or metric for short, defines the geometric and causal structure of the spacetime. Physical distances for nearby points are measured via the line element, written in Einstein summation convention as

$$ds^2 = g_{\alpha\beta}\, dx^\alpha dx^\beta, \tag{1.1}$$

with $g_{\alpha\beta}$ the metric tensor and $dx^\alpha$ an infinitesimal coordinate displacement. The metric tensor is assumed to be symmetric in GR, that is $g_{\alpha\beta} = g_{\beta\alpha}$ [3]. Indices are summed over $\alpha = 0, 1, 2, 3$, with 0 indicating the time coordinate. For Minkowski spacetime, the 4-vector is defined as $dx^\alpha = (-cdt, dx, dy, dz)$, which is given in the metric signature $(-+++)$ that will be used consistently throughout this work.

The inverse metric $g^{\beta\gamma}$ is defined by the product $g_{\alpha\beta}\, g^{\beta\gamma} = g^{\gamma\beta}\, g_{\beta\alpha} = \delta^\gamma_\alpha$, with $\delta^\gamma_\alpha$ the Kronecker delta, which is defined as

$$\delta^\nu_\mu = \begin{cases} 1 & \text{for } \alpha = \gamma \\ 0 & \text{for } \alpha \neq \gamma. \end{cases} \tag{1.2}$$

The metric and its inverse are then used to raise and lower indices on a tensor, for example $T^{\alpha\beta}{}_{\gamma} = g_{\lambda\gamma}\, T^{\alpha\beta\lambda}$.

The causal structure of spacetime is then given by the sign of the line element; for $ds^2 < 0$, $dx^\alpha$ is a timelike interval, for $ds^2 = 0$ it is a null interval or lightlike interval, and for $ds^2 > 0$ $dx^\alpha$ is a spacelike interval. This translates as for an event with a given set of coordinates within the spacetime, only events within its light cone (defined by the null curves) can have an influence on that point. Events outside the null cone cannot affect the event as they are out of causal contact. An example of a spacelike curve is the edge of a table at a given moment in time. Thus all massive particles follow timelike curves as they cannot exceed the speed of light and massless particles follow null curves.

### 1.2.2 Curvature

As the metric defines the geometry of spacetime, it completely determines the curvature of spacetime. First, the concept of a derivative must be extended to tensors in a way that preserves the properties of a tensor. This is the covariant derivative $\nabla_\alpha$, which when applied to a tensor $T^\beta$ gives

$$\nabla_\alpha T^\beta = \partial_\alpha T^\beta + \Gamma^\beta{}_{\alpha\gamma} T^\gamma. \tag{1.3}$$

The term $\Gamma^\beta{}_{\alpha\gamma}$ is known as the connection. In GR, in order to preserve features of Euclidean geometry in general coordinates, the covariant derivative of the metric is zero, $\nabla_\alpha g_{\beta\gamma} = 0$ [3]. This is known as metric compatibility and allows for the connection to be defined in terms of the metric as

$$\Gamma^\alpha{}_{\gamma\delta} = \frac{1}{2} g^{\alpha\beta}(\partial_\delta g_{\beta\gamma} + \partial_\gamma g_{\delta\beta} - \partial_\beta g_{\gamma\delta}). \tag{1.4}$$

This special case of the connection is called the Christoffel symbol and due to the symmetry of the metric, it too is symmetric, $\Gamma^\alpha{}_{\gamma\delta} = \Gamma^\alpha{}_{\delta\gamma}$.

A geodesic is a curve in spacetime that is the shortest distance between two points, thus representing a "straight" line for that spacetime. As an example, for two points on the surface of a 2-sphere, the geodesic connecting them is the great circle through those points. Though in this case, both the shortest and longest lines connecting these points are geodesics. So it is more correct to say that a geodesic maximes the proper time for a timelike geodesic, or maximises the proper length for a spacelike geodesic. Null paths

are always geodesics. The geodesic equation is

$$X^\beta \nabla_\beta X^\alpha = \frac{d^2x^\alpha}{dv^2} + \Gamma^\alpha{}_{\beta\gamma}\frac{d^2x^\beta}{dv^2}\frac{d^2x^\gamma}{dv^2} = 0, \tag{1.5}$$

where $X^\alpha = d^\alpha/dv^2$. $v$ is the curve parameter; in GR it typically represents proper time, or proper distance if the curve is spacelike. The importance of geodesics to GR are that they represent the motion of freely moving particles and of pressure free matter. The Christoffel symbols represent inertial forces in flat space, which can be seen by transforming into rotating coordinates. Since the equivalence principle states that inertia and gravity are locally indistinguishable, this means that both gravitational and inertial forces are incorporated into $\Gamma^\alpha{}_{\beta\gamma}$. This gives the conclusion that gravity is not a force, but is instead an inertial property of matter freely falling in curved spacetime [3].

The Riemann tensor (or curvature tensor) is then given in terms of the Christoffel symbols as

$$R^\alpha{}_{\beta\gamma\delta} = \partial_\gamma \Gamma^\alpha{}_{\delta\beta} - \partial_\delta \Gamma^\alpha{}_{\gamma\beta} + \Gamma^\alpha{}_{\gamma\lambda}\Gamma^\lambda{}_{\delta\beta} - \Gamma^\alpha{}_{\delta\lambda}\Gamma^\lambda{}_{\gamma\beta}. \tag{1.6}$$

Therefore, the curvature of the space is derived from the second derivative of the metric. The structure of Einstein's Field Equations can now be obtained from the Riemann tensor. First, cyclic covariant derivatives of the Riemann tensor give the Bianchi Identities [4]

$$\nabla_\lambda R_{\alpha\beta\gamma\delta} + \nabla_\delta R_{\alpha\beta\lambda\gamma} + \nabla_\gamma R_{\alpha\beta\delta\lambda} = 0. \tag{1.7}$$

Contracting twice over Eq. (1.7) gives

$$0 = g^{\alpha\gamma} g^{\beta\delta}(\nabla_\lambda R_{\alpha\beta\gamma\delta} + \nabla_\delta R_{\alpha\beta\lambda\gamma} + \nabla_\gamma R_{\alpha\beta\delta\lambda}) \tag{1.8}$$

$$0 = \nabla_\lambda R - \nabla_\delta R^\delta{}_\lambda - \nabla_\gamma R^\gamma{}_\lambda \tag{1.9}$$

$$0 = \nabla_\delta R\, \delta^\delta_\lambda - 2\nabla_\delta R^\delta{}_\lambda \tag{1.10}$$

$$0 = \nabla_\delta (R^\delta{}_\lambda - \frac{1}{2} R\, \delta^\delta_\lambda), \tag{1.11}$$

which is analogous to $\nabla_\nu G^{\mu\nu} = 0$, with

$$G^{\mu\nu} = R^{\mu\nu} - \frac{1}{2} R\, g^{\mu\nu} \tag{1.12}$$

the Einstein tensor.

### 1.2.3 The Einstein Field Equations

Thus far only the geometry of spacetime has been described; the matter and energy content still has to be defined. This is done through the energy-momentum tensor $T^{\mu\nu}$. This

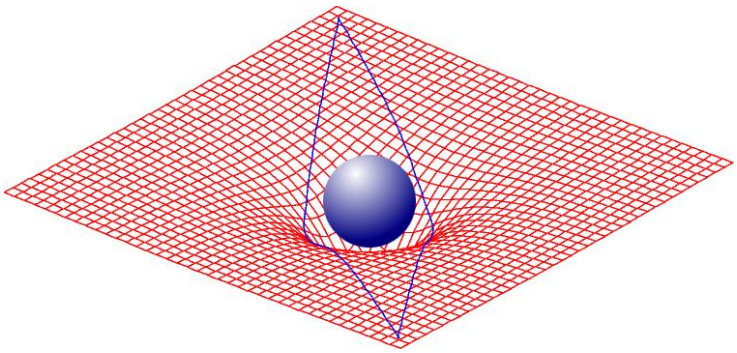

Figure 1.1: Mass curves the spacetime around it, which in turn causes the path of the light rays to deflect inwards towards the mass. Figure taken from [5]

tensor describes the flux of 4-momentum $p^\mu$ in spacetime orthogonal to the $x^\nu$ direction [6]. From the minimal coupling condition, which is the assumption that known physics in flat spacetime can be rewritten in covariant form in curved spacetime through simple transitions, i.e. $\partial_\mu \Rightarrow \nabla_\mu$, it can be proved that $\nabla_\nu T^{\mu\nu} = 0$ [4]. Thus local energy and matter is conserved.

From the conservation or energy, and given that $\nabla_\nu G^{\mu\nu} = 0$, this allows for spacetime and energy to be linked through the Einstein Field Equations (EFE)

$$G^{\mu\nu} = R^{\mu\nu} - \frac{1}{2} R\, g^{\mu\nu} = \frac{8\pi G}{c^4} T^{\mu\nu}, \tag{1.13}$$

with the constant before the energy-momentum tensor determined by the Newtonian limit. The EFE's tell spacetime how to behave in the presence of energy and matter, and vice versa. Matter and energy curve the spacetime around it, which in turn determines the path matter can travel in that spacetime, as demonstrated in Figure 1.1.



## 1.3 The Friedmann-Lemaître-Robertson-Walker Model

The standard model of cosmology is the Friedmann-Lemaître-Robertson-Walker (FLRW) model. It assumes a spatially homogenous, isotropic universe, and is the only model that fulfills those conditions. The metric was derived only from the conditions of homogeneity and isotropy [7, 8], and the EFE's are only needed to derive the scale factor of the Universe as a function of time.

The assumption of isotropy is that the Universe is invariant under spatial rotation, that is, it looks the same in all directions. Homogeneity is that the Universe is invariant

under spatial translation; that the Universe is the same at all points and that the laws of physics are identical at all points in the Universe. On small scales, the Universe does not look the same at different locations due to the clustering of matter, but at larger scales on the order of gigaparsecs, the Universe does appear to be uniform in composition.

### 1.3.1 The FLRW metric

In units defined such that $c = 1$, the line element for the FLRW model is defined to be [9]

$$ds^2 = -dt^2 + a(t)^2 \left( \frac{dr^2}{1 - kr^2} + r^2(d\theta^2 + \sin^2 \theta d\phi^2) \right). \tag{1.14}$$

$a(t)$ is the scale factor of the Universe and represents the relative expansion of the Universe. It does this through relating the proper distance between two points at some arbitrary time $t$ to the distance between them at a reference time $t_0$ through the expression

$$d(t) = a(t)d_0 \tag{1.15}$$

with $d(t)$ the proper distance at time $t$, and $d_0$ the distance at reference time $t_0$. The scale factor is thus a function of time only, otherwise it would violate the conditions of homogeneity and isotropy. The distance coordinate $r$ in Eq. (1.14) has been rescaled so that the curvature parameter $k$ now takes values of -1, 0, +1 for open, flat and closed universes respectively.

### 1.3.2 The Evolution Equations

Energy and matter in the Universe is typically modelled as a perfect fluid. The reason for this is that perfect fluids are irrotational, have no shear stresses or viscosity, and are isotropic in their rest frames; which is how large scale matter and energy distribution in a homogenous and isotropic universe affected only by gravitational interactions is expected to behave. The energy-momentum tensor for a perfect fluid is given as [10]

$$T^{\mu\nu} = \begin{pmatrix} -\rho & 0 & 0 & 0 \\ 0 & p & 0 & 0 \\ 0 & 0 & p & 0 \\ 0 & 0 & 0 & p \end{pmatrix}. \tag{1.16}$$

Taking the 00-component of the conservation equation, $\nabla_\nu T^{\mu\nu} = 0$, as it is applied to Eq. (1.16) gives

$$\dot{\rho} + 3(\rho + p)\frac{\dot{a}}{a} = 0, \tag{1.17}$$

with the overdot indicating the derivative with respect to proper time. As an aside, since the scale factor measures the relative expansion of the Universe, it can be related to volume. Multiplying Eq. (1.17) by $a^3$ and assuming that $a^3 \propto V$ gives

$$\frac{\partial}{\partial t}(\rho V) + p\frac{\partial}{\partial t}V = 0, \tag{1.18}$$

and as $E = \rho V$, this converts Eq. (1.18) to $dE + pdV = 0$, the First Law of Thermodynamics.

Taking the 00-component of the EFE's, Eq. (1.13), as it is applied to a perfect fluid gives

$$\left(\frac{\dot{a}}{a}\right)^2 = \frac{8\pi G}{3}\rho - \frac{k}{a^2}, \tag{1.19}$$

which is the Friedmann equation. The trace of the EFE's is the Raychaudhuri equation [6]

$$\frac{\ddot{a}}{a} = -\frac{4\pi G}{3}(\rho + 3p). \tag{1.20}$$

Solving for these two expressions will give Eq (1.17), the conservation of mass-energy. The Friedmann equation relates to the expansion rate of the Universe, also known as the Hubble parameter, via

$$H \equiv \frac{\dot{a}}{a}, \tag{1.21}$$

leading to the left hand side of Eq. (1.20) being equivalent to $\dot{H} + H^2$.

### 1.3.3 The Hubble Parameter

Consider a barotropic fluid, which is a perfect fluid that has a linear relationship between pressure and density, $p = w\rho$. Substituting this relationship into the conservation equation, Eq. (1.17) gives

$$\frac{\dot{\rho}}{\rho} = -3(1 + w)\frac{\dot{a}}{a}, \tag{1.22}$$

which can be integrated to give [11]

$$\rho \propto a^{-3(1+w)}. \tag{1.23}$$

$w$ is the equation of state parameter of the fluid and will change depending upon the type of fluid being considered. For a collisionless fluid, which is defined as all particles interacting only through gravitational effects, $w = 0$. This is also known as dust and

results in Eq. (1.23) becoming $\rho \propto a^{-3}$. Similarly, radiation with $w_{rad} = 1/3$ gives $\rho_{rad} \propto a^{-4}$. Therefore, the total density of the fluid is

$$\rho = \sum^{n} \rho_i \, a^{-3(1+w_i)}. \tag{1.24}$$

Substituting this into the Friedmann equation, Eq. (1.19) will give

$$H^2 = \frac{8\pi G}{3} \sum^{n} \rho_i \, a^{-3(1+w_i)} - \frac{k}{a^2}, \tag{1.25}$$

which can be converted to

$$H^2 = H_0^2 \left( \frac{8\pi G}{3H_0^2} (\rho_R a^{-4} + \rho_M a^{-3}) - \frac{k}{a^2 H_0^2} \right), \tag{1.26}$$

with $\rho_R$ and $\rho_M$ the densities of radiation and matter at current times respectively, and $H_0$ is the Hubble constant, the current value for the Hubble parameter. Radiation is defined to be photons and particles moving at relativistic speeds whilst matter is baryonic matter and dark matter. Defining the critical energy density of flat space to be

$$\rho_{crit} = \frac{3H_0^2}{8\pi G} \tag{1.27}$$

allows for the density parameter to be defined as

$$\Omega = \frac{\rho}{\rho_{crit}}. \tag{1.28}$$

Eq (1.26) then becomes

$$H^2 = H_0^2 \left( \Omega_R a^{-4} + \Omega_M a^{-3} - \frac{k}{a^2 H_0^2} \right). \tag{1.29}$$



Homogeneity and isotropy dictate a spatial geometry with a constant curvature, meaning that the global distribution of energy and matter would lead to a global curvature of spacetime. Thus the density parameter $\Omega$ is related to the curvature of spacetime, which is why the critical energy density is defined for flat space. By definition, the density of all matter and energy in a flat universe should add up to unity,

$$\Omega = 1 = \sum^{n} \Omega_i. \tag{1.30}$$

In the event that the density of matter is more or less than the critical density, spacetime will be curved. If $\Omega < 1$ then there is negative curvature, and if $\Omega_K > 0$ there is positive curvature. Cosmic curvature is defined through the curvature density parameter,

$$\Omega_K = 1 - \sum^{n} \Omega_i = -\frac{k}{a^2 H_0^2}. \tag{1.31}$$

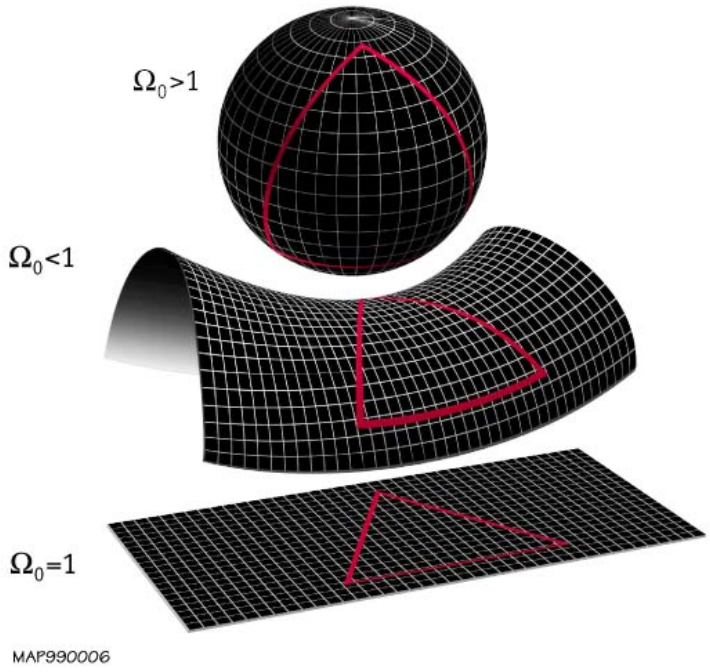


Figure 1.2: **Geometry of the Universe** In a flat universe, parallel lines remain parallel till infinity and the sum of the angles of a triangle in this geometry add up to 180°. In a closed universe, parallel lines will not remain so but will converge and eventually meet. This causes triangles to have angles summing to more than 180°. Conversely, an open universe will have parallel lines that diverge, and triangles that have interior angles that sum to less than 180°. Figure taken from [12].

Therefore, $k = 0$ gives flat space, $k = -1$ gives $\Omega_K > 0$ and $k = +1$ gives $\Omega_K < 0$. In this way, the curvature density either subtracts energy from or adds energy to the flat case to give a curved geometry. Positive curvature is thus defined by a negative curvature density to remove excess energy to give the flat space dynamics whilst negative curvature has a positive curvature density to add energy to the system. A positively curved universe is defined by spherical geometry and is called "closed", a "flat" universe is given by Euclidean geometry and a negatively curved universe is determined by hyperbolic geometry and is refered to as "open". The geometry of the Universe has consequences for the paths of light rays through it, as described in Figure 1.2.

Curvature can be related back to the scale factor in the following fashion; the three-dimensional Ricci scalar is given as

$$ {}^3R = \frac{6k}{a(t)^2}, \tag{1.32}$$

which is the spatial curvature of the universe. In order that the curvature parameter $k$ could be rescaled as +1, 0, -1, the original distance parameter $r$' was rescaled in the construction of the FLRW model to be the dimensionless coordinate distance $r$, defined as [13]

$$r \equiv \frac{r'}{a(t)}. \tag{1.33}$$

In this fashion, the scale factor thus becomes the radius of the space that was defined, either the radius of a sphere in a closed universe, or an imaginary radius in the open case. Extending the scale factor to infinity will reduce the metric to the flat case. Given that

$$\Omega - 1 = \frac{k}{H^2 a^2}, \tag{1.34}$$

it is clear that the Ricci scalar can be expressed as

$$R = 6H^2(\Omega - 1). \tag{1.35}$$

From the form of the FLRW metric, specifically the $1/(1-kr^2)$ term, the effects of spatial curvature become very important when $r \sim |k|^{-1/2}$. This allows us to define a physical radius of curvature for the universe,

$$R_{curv} \equiv a(t)|k|^{-1/2} = \sqrt{\frac{6}{|R|}} \tag{1.36}$$

which is related to the Hubble radius, $H^{-1}$, by [13]

$$R_{curv} = \frac{H^{-1}}{|\Omega - 1|^{1/2}}. \tag{1.37}$$



A note on the nomenclature; whilst the terms open and closed refer to negative and positive curved universes, these terms are ambiguous as they are derived from the terms used for topological sets. Mathematically, for the universe to be infinite or finite in extent, it would have to be either an unbounded or bounded metric space, respectively. An unbounded metric space means that there exist points that are arbitrarily far apart; for any distance $d$ in this space there will exist points that are seperated by a distance greater than $d$. A bounded space conversely will have a distance $d$ such that all points in the space are within the distance $d$ from each other. Further, a bounded space can be defined as compact, meaning that there will exist closed geodesics. An example of a closed geodesic is a great circle on a sphere; it begins as a straight line that if extended far enough in one direction it will reach its starting point. Spherical geometry is compact,

whilst flat and hyperbolic geometry can be either compact or unbounded. Examples are Euclidean space, which is flat and infinite, and a torus, which is flat yet compact. Therefore a closed universe refers to a compact, bounded geometry whilst open and flat could refer to either bounded or infinite universes, though they typically refer to the infinite case.

Dark energy is a recent phenomenon in cosmology, only having been discovered in 1998 [14, 15]. Dark energy is what is believed to be causing the accelerated expansion of the Universe at late times. One early model was that of a cosmological constant $\Lambda$. This leads to Einstein's Field Equations Eq. (1.13) being modified to

$$G^{\mu\nu} = R^{\mu\nu} - \frac{1}{2}R\, g^{\mu\nu} = \frac{8}{c^4}T^{\mu\nu} - \Lambda g^{\mu\nu}. \tag{1.38}$$

This is the cosmological constant that Einstein originally inserted to prevent expansion of the Universe and keep it in a steady state. Now it is modelled as a negative pressure that drives the expansion of the Universe. After adding it to the EFE's, the Friedmann and Raychaudhuri equations now have an added $+\Lambda/3$ term. Further, the equation of state parameter for $\Lambda$ is $w = -1$, i.e. $p = -\rho$, which leads to a new form of the Hubble Parameter, Eq. (1.29),

$$H^2 = H_0^2 \left(\Omega_R a^{-4} + \Omega_M a^{-3} + \Omega_K a^{-2} + \Omega_\Lambda\right). \tag{1.39}$$

However, a more general form of dark energy is modelled as $\Omega_{DE}$,

$$H^2 = H_0^2 \left(\Omega_R a^{-4} + \Omega_M a^{-3} + \Omega_K a^{-2} + \Omega_{DE} f(z)\right), \tag{1.40}$$

where $f(z)$ is

$$f(z) = \exp\left[3\int_0^z \frac{1 + w(z')}{1 + z'} dz'\right], \tag{1.41}$$

the evolution of dark energy with redshift, $z$. In this case, the equation of state parameter is now a function of redshift. This, combined with replacing $a(t)$ with $(1+z)^{-1}$ (discussed in the next section) in Eq. (1.40) gives the final expression for the Hubble Parameter

$$H(z)^2 = H_0^2 \left(\Omega_R(1+z)^4 + \Omega_M(1+z)^3 + \Omega_K(1+z)^2 + \Omega_{DE} f(z)\right). \tag{1.42}$$

## 1.4 Measuring the Universe

Having introduced the mathematical and theoretical tools that are used to model the Universe, the observational methods used to measure and quantify the Universe must

now be defined. The Universe can be measured in a variety of ways; observations of the electromagnetic spectrum and gravitational waves, as well as of neutrinos and other high energy particles. Currently, gravitational waves are incredibly difficult to detect, whilst neutrino measurements are mainly for studying our Sun. This leaves light rays as the primary method of measuring our Universe, with wavelengths ranging from gamma rays and X-rays to radio waves. The tools used to interpret optical measurements are developed in the next few sections, as well as how observations are married to the theory developed earlier.

### 1.4.1 Redshift

When astronomical objects are observed via the electromagnetic spectrum, one of the quantities measured is its redshift. When electromagnetic radiation has been redshifted, the wavelength of any given light ray increases; for visible light it becomes "redder" as it shifts towards the red end of the visible spectrum which is what gives this phenomenon its name. One way in which electromagnetic radiation can be redshifted is if the source and observer are moving away from each other, leading to the spectrum being Doppler shifted. However, in cosmological terms, the redshift that galaxies display is due to the metric expansion of space, i.e. the space between galaxies is increasing, leading to a decrease of the energy of the light rays travelling between them. Light can also be redshifted through gravitational effects, though for the purposes of this text, only the expansion case will be considered.



The redshift $z$ is defined to be the fractional change in the wavelength of light [9]

$$1 + z = \frac{\lambda_{obs}}{\lambda_{emit}}, \tag{1.43}$$

where $\lambda_{obs}$ and $\lambda_{emit}$ are the observed and emitted wavelengths of light respectively. This can be related to the scale factor, and subsequently the expansion of space by solving for the FLRW metric on null geodesics; $ds^2 = 0$ for null geodesics, and they travel on radial paths, so $d\theta = d\phi = 0$. This gives Eq. (1.14) as

$$ds^2 = 0 = -dt^2 + a(t)^2 \frac{dr^2}{1 - kr^2}. \tag{1.44}$$

Consider photons being emitted from a source at time $t_1$ with constant interval $\delta t_1$, and those same photons being observed now at time $t_0$ with interval $\delta t_0$. These quantities can be related to each other and the expansion of space via [9]

$$\frac{\delta t_1}{a(t_1)} = \frac{\delta t_0}{a_0}. \tag{1.45}$$

Using this information, Eq. (1.44) can be solved to give

$$1 + z = \frac{a_0}{a(t)}. \tag{1.46}$$

By definition $a_0$, being the current scale of the Universe, is taken to be 1. Then Eq. (1.46) becomes $a(t) = (1 + z)^{-1}$.

### 1.4.2 Distance Measurements

The redshift of light is now used to determine the distance to objects in the Universe. For objects that are considered close, with redshift $0.05 < z \ll 1$, Hubble's Law applies

$$v = H_0 d. \tag{1.47}$$

$v$ is the recessional velocity and $d$ is the distance to the object, given in megaparsecs (Mpc). $H_0$ is the value of the Hubble parameter at current times and has units of inverse time, though is normally written as [16]

$$H_0 = 100h\,\mathrm{km\,s^{-1}\,Mpc^{-1}}, \tag{1.48}$$

with $h$ being a dimensionless constant that parametrizes values of the Hubble constant. This leads to two other relations; the inverse of the Hubble constant gives Hubble time

$$t_H = \frac{1}{H_0}, \tag{1.49}$$

and when the speed of light is multiplied by the Hubble time, the Hubble distance is defined

$$d_H = \frac{c}{H_0}. \tag{1.50}$$



For larger redshifts, the geometry of the Universe affects the distance measured. This is due to the matter and energy content curving the spacetime that the geodesics propagate through. Distances in this case are typically measured in comoving coordinates. Since space is expanding, comoving coordinates are used to measure the coordinate distance between points. Using a sphere as an example; for an observer located at the origin, any two points fixed on the surface of the sphere can be measured in parameters $(r, \theta, \phi)$. Should the sphere expand or contract, the distance between the points in the sphere will change, whilst the coordinates measured by the observer will remain constant. Thus the coordinates are comoving with the expansion of the space. Another example is given in

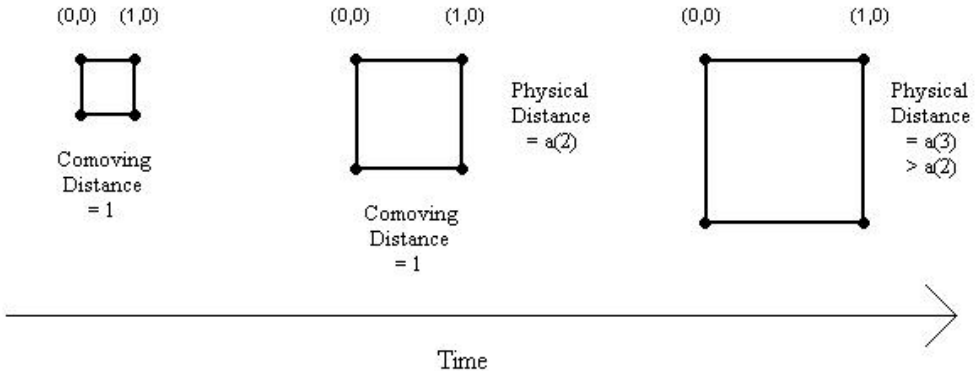


Figure 1.3: **Comoving coordinates** As space expands uniformly points on a grid will expand with it. The coordinates for the points will remain the same and so the coordinate distance will remain constant, but the physical distance, which is related to the scale factor, will increase with time. Figure adapted from [10].

Figure 1.3.

For larger redshifts, the line-of-sight or radial comoving distance is defined to be [16]

$$d_R(z) = \frac{c}{H_0}\int_0^z \frac{dz'}{E(z')}, \tag{1.51}$$

where $E(z)$ is the dimensionless Hubble parameter

$$E(z) \equiv \frac{H(z)}{H_0} = \sqrt{\Omega_M(1+z)^3 + \Omega_K(1+z)^2 + \Omega_{DE}f(z)} \tag{1.52}$$

with $f(z)$ as defined in Eq. (1.41). The transverse comoving distance is

$$d_T(z) = \begin{cases} \frac{c}{H_0}\frac{1}{\sqrt{\Omega_K}}\sinh\left(\sqrt{\Omega_K}\int_0^z \frac{dz'}{E(z')}\right) & \text{for } \Omega_K > 0 \\ \frac{c}{H_0}\int_0^z \frac{dz'}{E(z')} & \text{for } \Omega_K = 0 \\ \frac{c}{H_0}\frac{1}{\sqrt{-\Omega_K}}\sin\left(\sqrt{-\Omega_K}\int_0^z \frac{dz'}{E(z')}\right) & \text{for } \Omega_K < 0. \end{cases} \tag{1.53}$$

From the transverse comoving distance two physical distances can be defined that are used to measure distances in the Universe; the angular diameter distance and the luminosity distance

$$d_L(z) = (1+z)d_T(z), \qquad d_A(z) = \frac{d_T}{1+z}. \tag{1.54}$$

These equations share the relationship $d_L(z) = (1+z)^2 d_A(z)$. The angular diameter distance does not increase to infinity like the luminosity distance does; instead it turns over at $z \sim 1$ resulting in more distant objects appearing to have a larger angular size as one looks back in time, as displayed in Figure 1.4 and Figure 1.5.

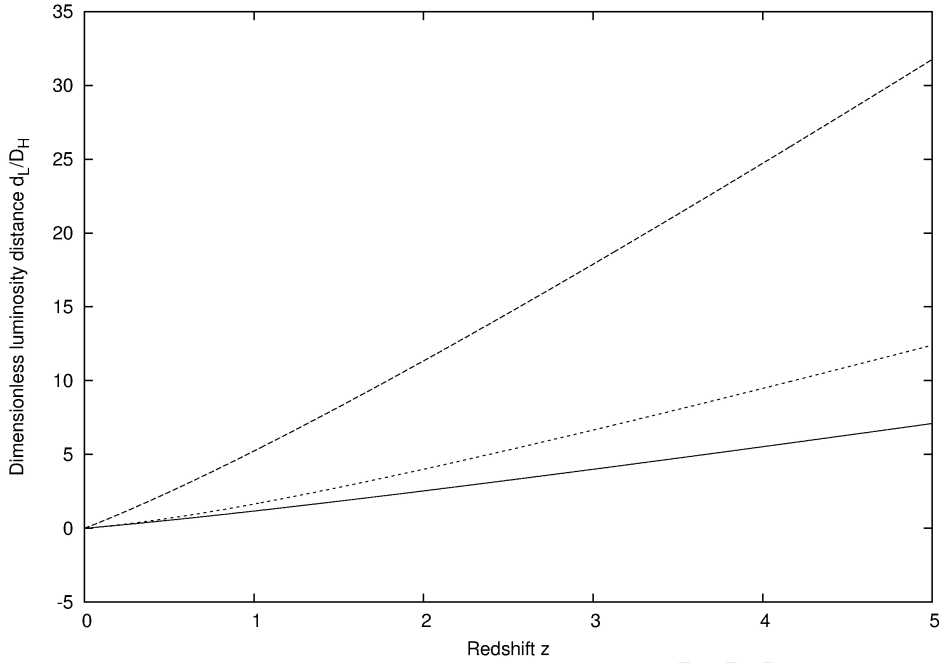


Figure 1.4: The dimensionless luminosity distance for three models; Einstein-de Sitter $(\Omega_M, \Omega_\Lambda) = (1.0, 0)$ for the solid line, low density (0.05, 0) for the long-dashed line, and high $\Lambda$ (0.2, 0.8) for the short-dashed line. Figure adapted from [16].

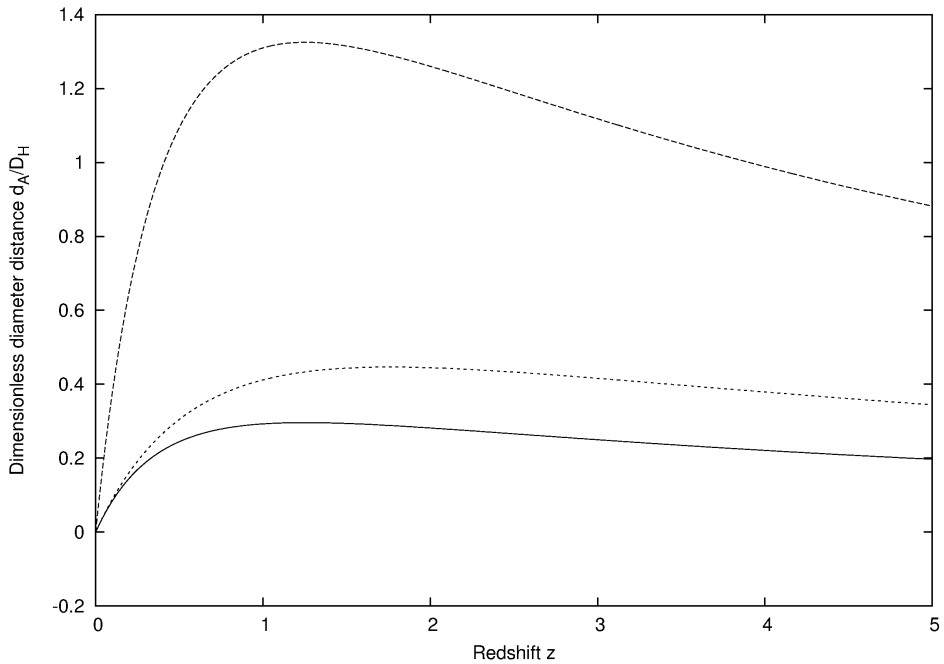


Figure 1.5: The dimensionless angular diameter distance for three models; Einstein-de Sitter $(\Omega_M, \Omega_\Lambda) = (1.0, 0)$ for the solid line, low density (0.05, 0) for the long-dashed line, and high $\Lambda$ (0.2, 0.8) for the short-dashed line. Figure adapted from [16].

## 1.5 Baryon Acoustic Oscillations

The Baryon Acoustic Oscillations (BAO) are a frozen imprint of matter distribution in the early Universe at the moment of recombination. Their importance in modern cosmology is as statistical standard rulers, allowing for cosmic parameters to be constrained.

### 1.5.1 Standard Rulers

A standard ruler is a familiar concept from everyday life. It is an object of known size that when observed at different distances, will have different angular sizes. Then using the relation

$$d = \frac{L}{\theta}, \tag{1.55}$$

with $L$ the physical size and $\theta$ the angular size, the distance $d$ can be calculated. This is the method that humans use unconciously to judge distance; one example is when another person is spotted, assuming the average human height to be 6 feet allows for the distance to this person to be estimated.

The BAO are statistical standard rulers, as they are a preferred scale in the clustering of matter in the Universe. As the BAO are formed primarily from linear physics, this scale can be calculated accurately and is then used as the physical size of the BAO. Observing this physical size as an angular size subtended across the sky will allow for the distance to the BAO to be determined. In this way, distances to different points in the Universe can be accurately measured for a cosmological model. The BAO aren't just measured in a transverse fashion, they can also be measured radially, and this allows for the Hubble parameter for that mean redshift to be calculated. And so the BAO can serve the double purpose of measuring distances in the Universe, as well as its expansion rate, as seen in Figure 1.6.

Due to the clustering of matter, the BAO are not physical objects that can be directly observed. Their signature is hidden in the clustering pattern and must be calculated statistically. This is done by measuring the distance between every single galaxy pair that is observed, allowing the scale to be measured in the correlation between the galaxies. Another method is to take the Fourier transform of the matter distribution and analyse the resulting power spectrum. Figure 1.7 displays the effect clustering has on the observation of the preferred scale.

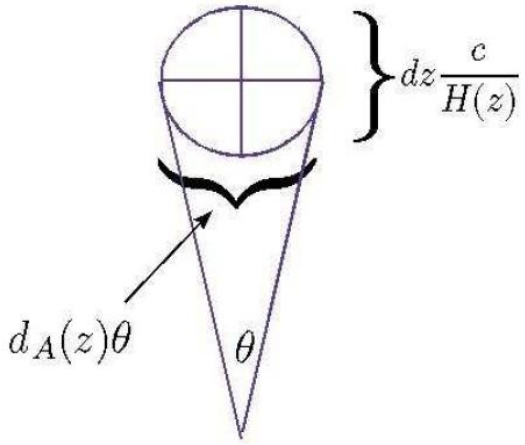


Figure 1.6: For a spherical object, the angular diameter distance $d_A(z)$ to it can be measuremed from its physical size $d_A(z)\theta$, whilst the radial distance is measured from $cdz/H(z)$, where $dz$ is the difference in redshift between the front and back points of the object and *H(z)* is the Hubble parameter. Figure from [17].



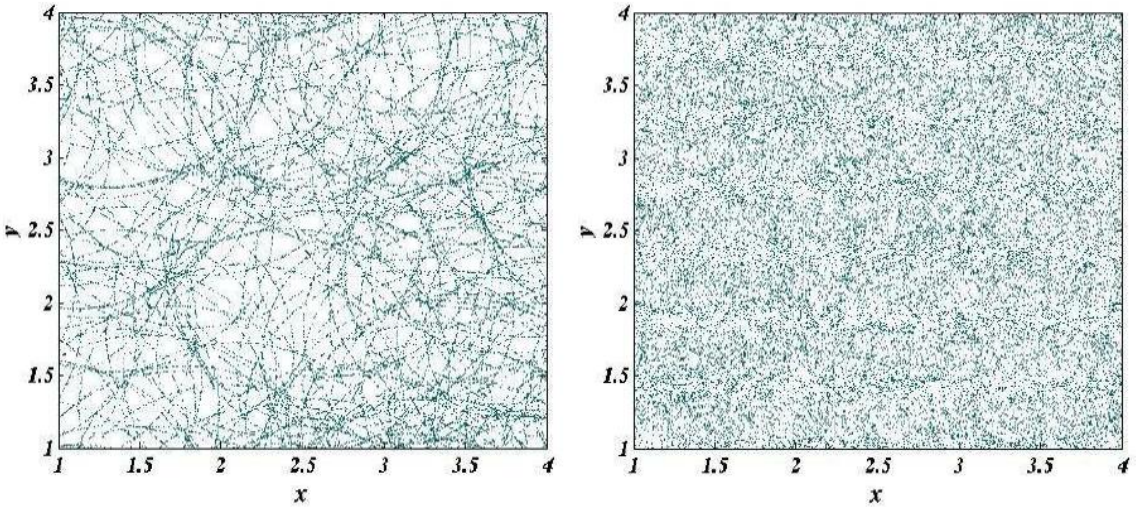


Figure 1.7: Points arranged on circles of fixed radius are placed in a given area. In the frame on the left, each circle contains many points and so the preferred scale of the objects can be easily observed. In the frame on the right, the same number of points are placed but now each circle only has a few points on it, and so the scale is hidden and must be extracted statistically. Figure from [17].

There are other statistical effects that can determine how accurate a measurement of the BAO scale is; cosmic variance and shot noise. The accuracy of the measurement is proportional to the fractional error of the power spectrum [18]

$$\frac{\delta P}{P} = \frac{1}{\sqrt{m}}\left(1 + \frac{1}{nP}\right), \tag{1.56}$$

where $P \equiv P(k^*)$, the power spectrum amplitude at an average scale $k^* \simeq 0.2h\,\mathrm{Mpc}^{-1}$ which is characteristic of the baryon oscillations. $m$ is the number of Fourier modes and $n$ is the number of points in the selection. The first term in Eq. (1.56) is the cosmic variance and the second term is the shot noise. Poisson shot noise is when there are too few points, leading to a large fractional error. As the density of points in the given volume is increased, the shot noise error will decrease. For astronomical surveys, to increase the number of targets will require longer integration times for a patch of sky, allowing the survey to probe deeper. This will result in a reduction of the area of sky being surveyed in a fixed observing time. Cosmic variance is the error that arises when the survey scale is smaller than the clustering scale. This means that large scale structure can only be observed in surveys that cover a volume much larger than the clustering scale. So to observe that BAO scale effectively, large sections of sky must be observed for long periods of time in surveys that will take years. This has been done in the Sloan Digital Sky Survey (SDSS) [19, 20] and is currently underway in the Baryon Oscillation Spectroscopic Survey (BOSS) [21].

### 1.5.2 Physics of the Baryon Acoustic Oscillations

In the early Universe all matter existed in the form of a hot, dense plasma of electrons, baryons and dark matter. All photons in the Universe were tightly coupled to the baryonic part of this plasma through Thompson scattering. For an overdense region of this plasma, the radiation pressure from the photons interacting with the baryonic part of the plasma causes the plasma to drive outwards. Counteracting this is the gravitational attraction due to the presence of the dark matter still forming the overdensity. This leads to oscillations in the plasma analogous to sound waves created in fluids via differences in pressure.

Consider one such acoustic wave emanating from an overdense region; the pressure would drive a spherical wave of baryons and photons outwards whilst dark matter would remain in the centre. After 380,000 years, or at a redshift of $z \approx 1{,}100$, the Universe cooled to a temperature of approximately 3000 K resulting in recombination, the forma-

tion of hydrogen from the baryonic elements of the plasma. As this matter is neutral, photons can no longer interact with it and are left to free stream through the Universe, becoming the Cosmic Microwave Background that is observed today. After recombination, the baryonic matter is left as a spherical shell around a region of dense dark matter. Due to gravitational attraction, the baryonic matter is attracted inward to the centre whilst the dark matter is attracted outward to the baryon shell, as displayed in Figure 1.8. Thus matter becomes more evenly distributed but with overdensities in the centre and at the shell, which is the sound horizon.

In the early Universe, the plasma contains many overdense regions. Each of these regions has a travelling acoustic wave emanate from it and then form as a shell around it. Due to the physics of galaxy formation, it is statistically more likely that a galaxy will form at one of these overdense regions. Thus galaxies are formed with an imprinted characteristic scale in their distribution.

The radius of this characteristic scale can be determined as follows; considering a single, spherical density perturbation travelling through the plasma with a sound speed

$$c_s = \frac{c}{\sqrt{3(1+R)}}, \tag{1.57}$$

where

$$R = \frac{3\rho_b}{4\rho_\gamma} \propto \frac{\Omega_b}{1+z}, \tag{1.58}$$

with $\rho_b$ and $\rho_\gamma$ the density of baryons and photons respectively. This sound wave will travel a distance

$$s = \int_{z_{rec}}^{\infty} \frac{c_s dz}{H(z)} = \frac{1}{\sqrt{\Omega_M H_0^2}} \frac{2c}{\sqrt{3 z_{eq} R_{eq}}} \ln \left[ \frac{\sqrt{1+R_{rec}} + \sqrt{R_{rec}+R_{eq}}}{1+\sqrt{R_{eq}}} \right], \tag{1.59}$$

where $z_{rec}$ stands for redshift at recombination, approximately 1,089, and $z_{eq} = \Omega_M/\Omega_R$ is the redshift of matter-radiation equality. The sound scale is thus calculated to be $\sim$ 148 Mpc, or $105h^{-1}$ Mpc. Though due to residual photon-baryon interactions after recombination the actual BAO scale might be slightly different. It has been suggested that $z_{rec}$ be replaced with $z_d = 1,019$, the drag epoch [23]. This gives the sound scale to be 155 Mpc, which is 5% larger than that calculated from the recombination history [24].

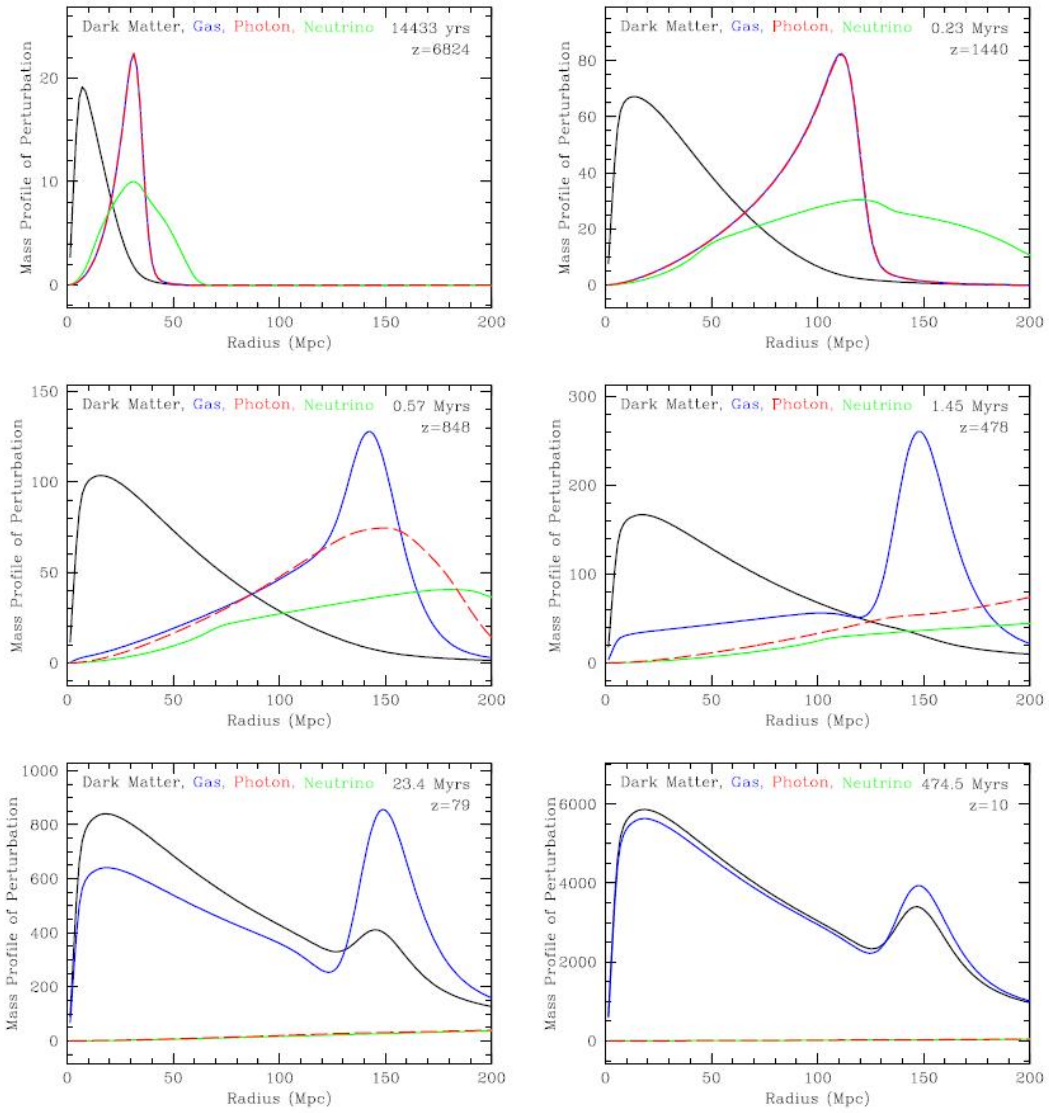


Figure 1.8: **An expanding spherical density perturbation** In these frames the black line represents the dark matter, red the photons, blue the baryonic matter and green the neutrinos. In the first frame (top left), there is an overdensity of matter located at the origin. Photons coupled to baryonic matter drive a density perturbation outwards from the origin whilst neutrinos are mostly gravitationally bound to the overdensity. In the second frame (top right) the expanding shell, having been driven a distance from the origin, attracts dark matter outwards through gravitational forces. Once recombination has occurred in frame three (middle left), the photons and neutrinos free stream away, leaving the baryonic matter as a shell around the overdensity. In subsequent frames, gravitational forces between the overdensity at the origin and the baryonic shell causes the distribution of matter to even out, leaving the signature that is detected today in frame six (bottom right). Figure taken from [22].

### 1.5.3 Observation of the Baryon Acoustic Oscillations

The BAO serve as statistical standard rulers in modern cosmology, being used to fix cosmic parameters. They do this in one of two ways; either by using the angular size of the BAO to determine distance via [17]

$$d_A(z) = \frac{s_\perp(z)}{\Delta\theta(1+z)}, \tag{1.60}$$

or the line-of-sight scale to determine the Hubble parameter and thus the expansion rate of the Universe,

$$H(z) = \frac{c\Delta z}{s_\parallel(z)}. \tag{1.61}$$

The BAO is refered to as a statistical standard ruler as it is not possible to directly observe the characteristic scale of the BAO in galaxy clustering; it must instead be measured via 2-point correlation measurements between every observable galaxy pair. The correlation function used is the Landy-Szalay estimator [25],

$$\zeta(r) = \frac{DD(r) - 2DR(r) + RR(r)}{RR(r)}, \tag{1.62}$$

with $D$ representing the data points and $R$ representing the random points. Thus $DD(r)$ is the distance measured between two galaxies from the data sample, $RR(r)$ are the distances between two galaxies in a catalogue of random galaxies with no preferred scale, and $DR(r)$ is the measurement between a galaxy in the data sample and one in the random catalogue. The BAO scale was first measured in 2005 from the analysis of a sample of 46,748 luminous red galaxies observed by the Sloan Digital Sky Survey, with a radius of $100h^{-1}$ Mpc [26]. The results are in Figure 1.9.



### 1.5.4 Developments in the Study of the Baryon Acoustic Oscillations

The current model for cosmology is the ΛCDM model, where CDM stands for Cold Dark Matter. The model is based on the FLRW model and assumes properties of the matter and energy content of the Universe. ΛCDM makes the following assumptions; the Universe is flat, homogenous and isotropic, there exists a cosmological constant that models the accelerated expansion of space, the Universe originated in an initial singularity or "Big Bang", and matter is composed of baryonic matter and cold dark matter. Cold dark matter is dark matter that is possibly non-baryonic, is non-relativistic (cold) and

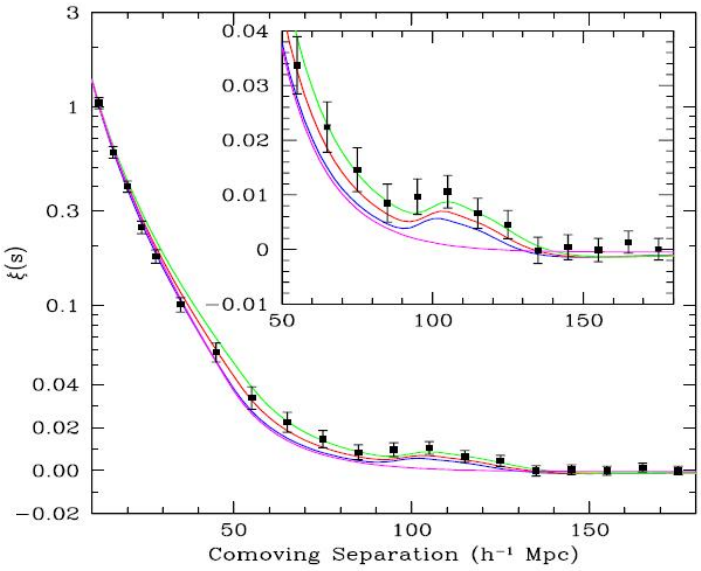


Figure 1.9: The BAO peak as detected by Eisenstein and his team in 2005. The models are $\Omega_M h^2 = 0.12$ (green), $\Omega_M h^2 = 0.13$ (red), and $\Omega_M h^2 = 0.14$ (blue). The magenta line is for a pure CDM model, $\Omega_M h^2 = 0.105$. Figure taken from [26].

only interacts gravitationally with itself and other matter. Table 1.1 contains the current parameter values for ΛCDM as measured from the Cosmic Microwave Background (CMB) by the Wilkinson Microwave Anisotropy Probe (WMAP) [27].

The BAO were first proposed in 1970 as the end result of a qualitative calculation that dealt with the collision equation of the photon distribution function [28]. The next mention of the BAO was as a proposal to explain the apparent excess clustering that was detected around $100h^{-1}$ Mpc, but was disregarded as too weak to be the cause of this excess [29]. Soon after, it was proposed in 1998 that the BAO can be used to measure cosmological parameters [30]. The modern ideas for the use of the BAOs was investigated in 2003 with the proposal that large-scale structure surveys and BAO be used as a standard ruler to fix cosmological parameters [31, 32, 33].

With the increased survey volume and number density of galaxies achieved in the 2dF and SDSS redshift surveys, the BAO peak was detected in 2005 [26] using the SDSS Data Release 3 (DR3) data, and later that year was detected in the 2dF survey [34]. BAO detections were subsequently used to constrain dark energy, curvature and the matter content of the Universe [34, 35, 36] for $z < 0.5$. CMB observations give the BAO scale

| Parameter | Value | Description |
|---|---|---|
| $t_0$ | $13.75 \pm 0.11 \times 10^9$ years | Age of the Universe |
| $H_0$ | $70.4^{+1.3}_{-1.4}\,\mathrm{km\,s^{-1}\,Mpc^{-1}}$ | Hubble constant |
| $\Omega_b$ | $0.0456 \pm 0.0016$ | Baryon density |
| $\Omega_c$ | $0.227 \pm 0.014$ | Dark matter density |
| $\Omega_\Lambda$ | $0.728^{+0.015}_{-0.016}$ | Dark energy density |
| $\Omega_K$ | $-0.0178 < \Omega_K < 0.0063$ | Curvature density |
| $\Omega_{tot}$ | $1.0023^{+0.0056}_{-0.0054}$ | Total energy density |

Table 1.1: Parameter values determined from the CMB as measured by WMAP. Table adapted from [27].

at $r = 153 \pm 2$ Mpc [27]. Measurements continued to be done giving ever more accurate results, using later SDSS data releases and a refined sample selection [37, 38].

Gaztañaga, Cabré & Hui used the SDSS DR6 and DR7 data releases to calculate the 2-point correlation function in both radial and perpendicular directions, finding a peak at $r \simeq 110h^{-1}$ Mpc [40]. The radial data enabled the first direct measurement of the Hubble parameter as a function of redshift $H(z)$, using the BAO peak as a standard ruler. Their results were $H(z = 0.24) = 79.69 \pm 2.32\,\mathrm{km\,s^{-1}\,Mpc^{-1}}$ for $z = 0.15 - 0.30$, $H(z = 0.43) = 86.45 \pm 3.27\,\mathrm{km\,s^{-1}\,Mpc^{-1}}$ for $z = 0.40 - 0.47$, and the whole sample of $z = 0.15 - 0.47$ gave $H(z = 0.34) = 83.80 \pm 2.96\,\mathrm{km\,s^{-1}\,Mpc^{-1}}$. Measurements such as this are accomplished through measuring the two-dimensional correlation function as in Figure 1.10.

The WiggleZ Dark Energy Survey [41, 42], combined with data from 6dFGS [43, 44] and SDSS was used to measure the BAO peak at $z = 0.44$, 0.6 and 0.73 [45]. Assuming a flat universe gave $w = -1.03 \pm 0.08$ and setting dark energy to be a cosmological constant found $\Omega_K = -0.004 \pm 0.006$.

Recent developments in the study of cosmological parameters using the BAO as a standard ruler used the SDSS Baryon Oscillation Spectroscopic Survey (BOSS) DR 9, which takes measurements in the redshift range $0.43 < z < 0.7$. The comoving angular diameter distance and the Hubble parameter were simultaneously constrained to be $2190 \pm 61$ Mpc and $94.4 \pm 4.5\,\mathrm{km\,s^{-1}\,Mpc^{-1}}$ respectively at $z = 0.57$ [46]. These results were used to produce a comoving angular diameter distance of $2094 \pm 34$ Mpc, which is

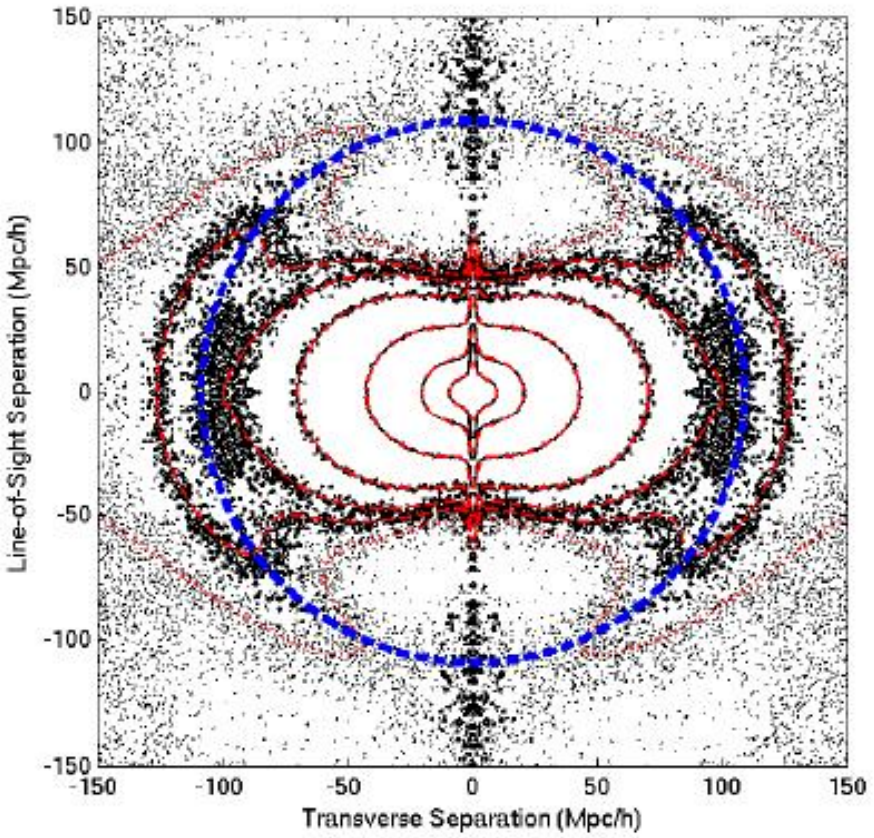


Figure 1.10: The spherically averaged two-dimensional correlation function measured from 160 SDSS LRG mock catalogues. The dashed blue line is the BAO scale. From this the radial and the transverse scales can be measured. Figure from [39]

claimed to be the most accurate result to date [47]. These results were then combined with CMB and SN Ia results to constrain cosmological parameters; $\Omega_M = 0.285 \pm 0.009$, $H_0 = 69.4 \pm 0.8\,\mathrm{km\,s^{-1}\,Mpc^{-1}}$, $\Omega_K = -0.0043 \pm 0.0049$ [48] and $\Omega_\Lambda = 0.74 \pm 0.016$ [46].

Whilst the BAO is normally measured with the 2-point correlation function, other means of measuring the location of the peak accurately have been proposed. Using a method first proposed in [49], the fitting formula for the first peak in the galaxy power spectrum is revised [50]. This uses the velocity overshoot effect, the idea that after recombination the different velocities of the baryons will cause the baryons to move kinematically, which creates a new perturbation in the baryon distribution. This is combined with a new recombination history to find the first peak in the matter power spectrum. These results are found to be consistent with those found in [23].

It was previously assumed that gravitational non-linear and redshift distortion effects would not shift the BAO peak, but would significantly affect the amplitude. Several simulations [51, 52, 53, 54, 22, 55] and analytical investigations [56, 57, 58, 22] were carried out with results indicating that radial measurements and the Hubble parameter will be less constrained than angular distance due to nonlinear redshift distortions.

Nishimichi *et al* [24] considered the effects that non-linear evolution and redshift-space distortions would have on the BAO peak in $k$-space. They investigated this numerically by contrasting the matter power spectrum against the smooth spectrum, taking the logarithmic derivative of the matter power spectrum, and contrasting with a linear approximation to the power spectrum given by Eisenstein & Hu in 1998 [23]. The first method is almost identical to what was proposed by Percival *et al* in 2007 [35]. The resulting data was then analysed for peaks and troughs which were compared against those from the linear theory in real space. The first method was found to be free of non-linear and redshift-space distortions, though overall the shifts in the peaks and troughs were on the order of $< 0.5\%$, with how much the peaks shifted being sensitive to the definition used for the BAO perturbation.

The first reconstruction of the acoustic peak took place in 2012, with reconstruction partially removing the effects of non-linear evolution and redshift distortions, resulting in a sharper acoustic peak [59]. Angular diameter distance was subsequently measured to be $d_A(z = 0.35) = 1050 \pm 38$ Mpc and the Hubble parameter to be

$H(z = 0.35) = 84.4 \pm 7.1\,\mathrm{km\,s^{-1}\,Mpc^{-1}}$. These results are a 1.4 times improvement in the error on $d_A(z)$ and a factor of 1.3 on the Hubble parameter. There was also an attempt to measure $H(z)$ and $d_A(z)$ from galaxy clustering data, without assuming a dark energy model or a flat universe [60]. The results were $H(z = 0.35) = 82.1^{+4.8}_{-4.9}\,\mathrm{km\,s^{-1}\,Mpc^{-1}}$ and $d_A(z = 0.35) = 1048^{+60}_{-58}$ Mpc.

N-body simulations have been used to study various effects that could change the position of the BAO peak. The effect of dark matter halo alignment on the correlation function was investigated [61]. Dark matter haloes are considered aligned when the dominant axes for the haloes are oriented with respect to each other, with significantly more correlation in haloes that are aligned parallel to each other. Also, haloes that are parallel to each other shift the BAO peak to smaller scales, whilst haloes that are perpendicular shift the peak to larger scales. Further, these simulations indicate that matter is anisotropically distributed beyond the BAO scale. Another study investigating the position of the BAO peak in overdense or underdense regions found that the scale shifted to smaller values in overdense regions [62]. This was attributed to the matter density causing the Universe to behave locally like a positively curved closed universe.

There has been discussion on using the BAO as a model independent test of cosmic expansion [63]. The proposed method is to compare the BAO scale at low and intermediate reshifts, with this test being independent of gravity, whether this be GR or any other model, the Friedmann equations, supernovae inferred distances and CMB observations. The test only assumes the Cosmological Principle and that the length scale of the BAO is fixed in comoving coordinates. This is coupled with a discussion of how combining $d_A(z)$ at different redshifts and current and future SN Ia surveys will break the degeneracy between curvature and dark energy history; further it alludes that combining the LRG and BAO data to CMB data will lower the uncertainty on curvature measurements. Lastly, it takes note of an argument that it is inappropriate to assume $\Omega_K = 0$ when constraining $w(z)$, as there is no experimental evidence that the Universe is flat unless $w(z) = -1$ is assumed [36].

In the future is the BigBOSS survey [64] which proposes to constrain early dark energy and curvature by measuring the Ly-$\alpha$ forest at $2.2 < z < 3.5$, a method which is also proposed in [65], in addition to targeting LRG's up to $z = 1$ and emission line galaxies up to $z = 1.7$. This will provide an expected 20 million galaxies with which to find the BAO

signal. Emission line galaxies offer a more accurate redshift reading than LRG's, yet due to their low bias a much higher density is required to do effective correlation calculations [17], which is why BigBOSS will be surveying much deeper for emission line galaxies than for LRG's. The Ly-$\alpha$ forest will provide a measurement of the acoustic signal in earlier times.

# Chapter 2

# Distances in a Curved Universe

Before studying the BAO in curved spacetimes, the distance measures must first be studied for differing cosmologies. In this chapter, the Hubble parameter $H(z)$ and the angular diameter distance $d_A(z)$ are studied for flat, open and closed universes. In this work, values used for calculations are given in Table 2.1 unless otherwise specified. The values were chosen to be close to the values determined by WMAP [27] yet were rounded off for simplicity in computation. The exception is the Hubble constant, which was chosen to sit evenly between the WMAP value $70.4^{+1.3}_{-1.4}\,\mathrm{km\,s^{-1}\,Mpc^{-1}}$ [27] and the value given in [66], $H_0 = 74.2 \pm 3.6\,\mathrm{km\,s^{-1}\,Mpc^{-1}}$, which was used as a prior in the calculation of the WMAP value. The chosen value for $|\Omega_K|$ is far larger than that calculated from the WMAP data; this is so any divergences from the flat case can be more easily identified.



## 2.1 The Hubble Parameter

The expansion history of the Universe is measured with the Hubble parameter

$$H(z)^2 = H_0^2 \left(\Omega_R(1+z)^4 + \Omega_M(1+z)^3 + \Omega_K(1+z)^2 + \Omega_{DE} f(z)\right). \tag{2.1}$$

| Parameter | Value |
|---|---|
| $H_0$ | $72.0\,\mathrm{km\,s^{-1}\,Mpc^{-1}}$ |
| $\Omega_M$ | 0.3 |
| $\Omega_{DE}$ | 0.7 |
| $\lvert\Omega_K\rvert$ | 0.05 |
| $w(z)$ | $-1$ |

Table 2.1: Fiducial parameter values used throughout this text.

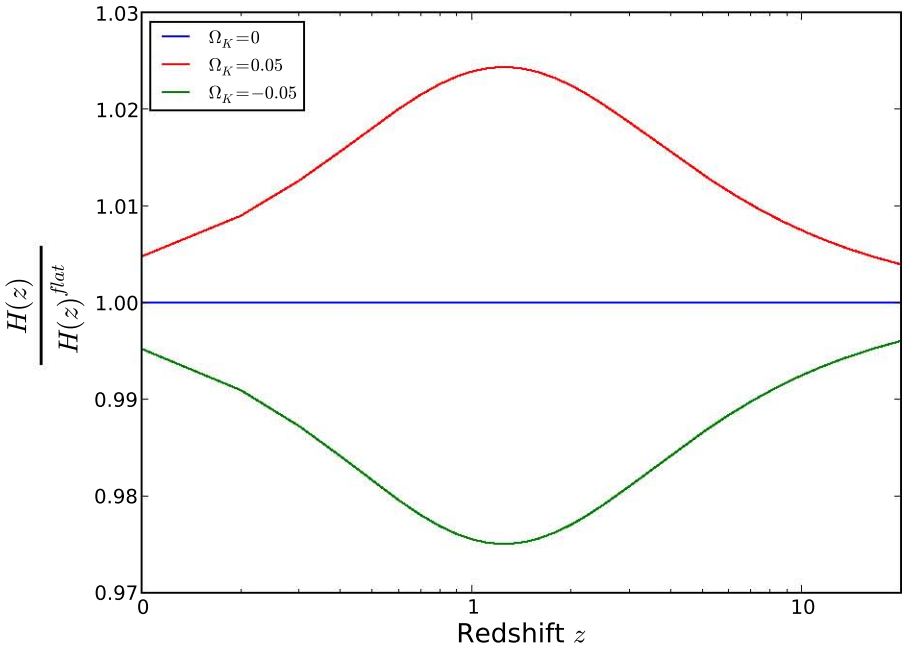


Figure 2.1: The Hubble parameter with $\Omega_M = 0.3$ and $\Omega_{DE}$ left to vary with curvature, $\Omega_{DE} = 1-\Omega_M-\Omega_K$. The open universe has the highest expansion rate and the closed universe the lowest.

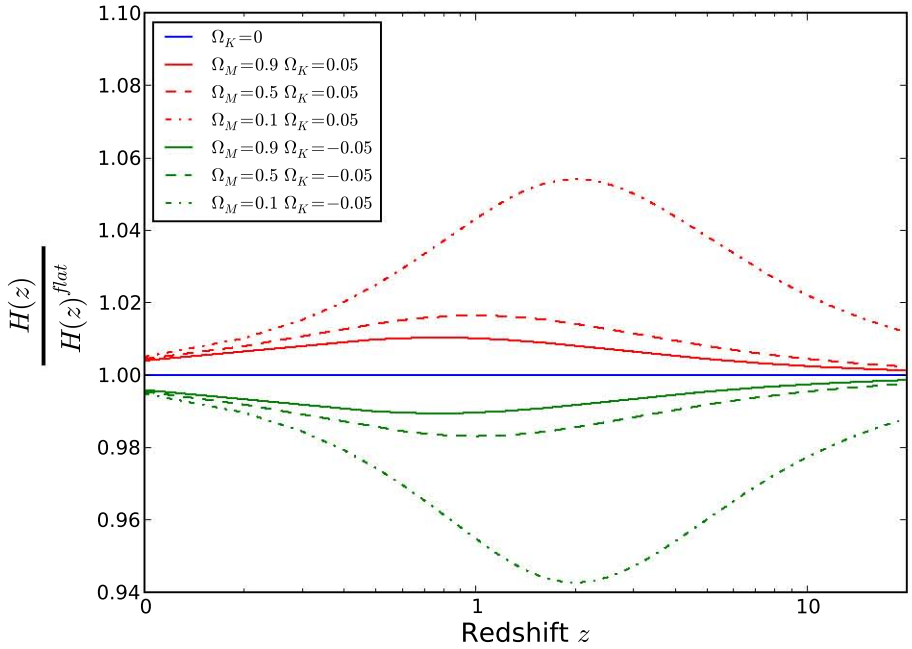


Figure 2.2: The Hubble parameter for universes with different matter densities. $\Omega_K = |0.05|$ for the curved models and $\Omega_{DE}$ was left to vary with curvature and $\Omega_M$. Open universes display the highest expansion rates and closed universes the lowest, with the lowest matter density models displaying the greatest differences from the fiducial model.

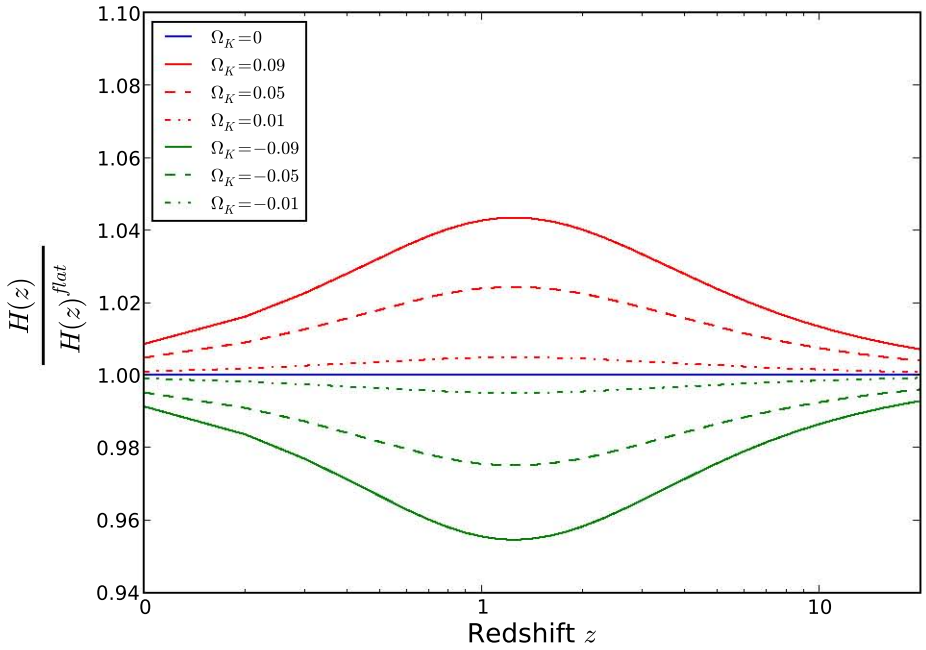


Figure 2.3: The Hubble parameter with $\Omega_M = 0.3$ and a changing $\Omega_K$, with dark energy density given by $\Omega_{DE} = 1 - \Omega_M - \Omega_K$.

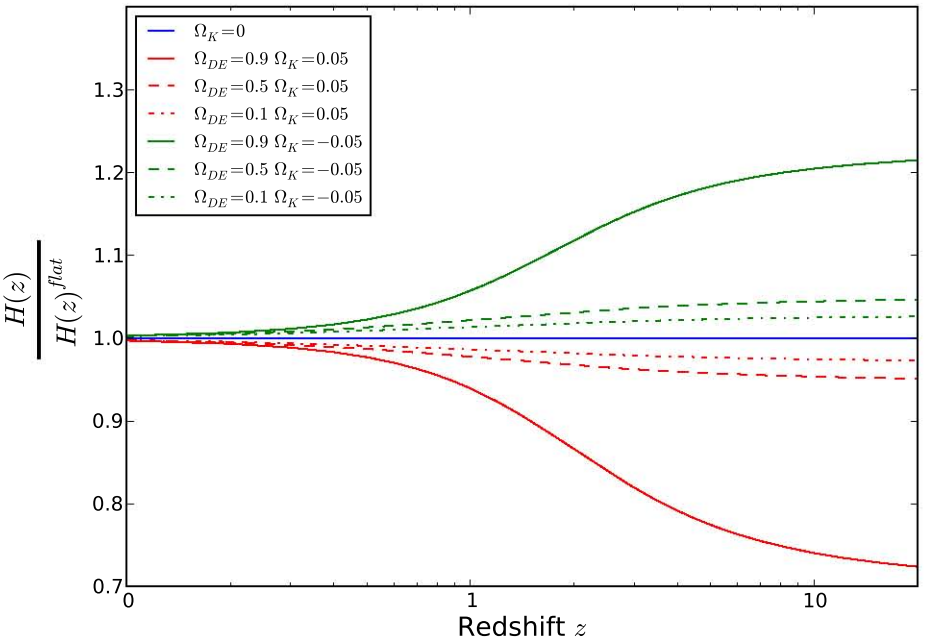


Figure 2.4: The Hubble parameter when dark energy density is fixed, $\Omega_K = |0.05|$ and matter density is left to vary, $\Omega_M = 1 - \Omega_{DE} - \Omega_K$. Closed universes now have the highest expansion rates due to the higher matter density present in these models and the increased dark energy leads to greater divergences from the fiducial model in earlier times.

To study how the Hubble parameter changes for different cosmologies, $H(z)$ was calculated for flat and curved universes and the amount of deviation from the flat model was calculated using the ratio of $H(z)/H(z)^{flat}$. $H(z)^{flat}$ is for a flat universe containing the fiducial values from Table 2.1. In order to keep total energy density at unity in the curved models matter density was fixed and dark energy was left to vary with curvature, $\Omega_{DE} = 1 - \Omega_M - \Omega_K$; though the equation of state parameter $w(z)$ was kept constant.

Figure 2.1 compares the Hubble parameter for open, closed and flat universes. As can be seen, an open universe would expand the quickest and a closed universe the slowest. When the same measurment is done for different matter densities, as in Figure 2.2, the results are consistent. However, for each cosmology, the lowest matter density causes the greatest difference from flat. This is due to the increased dark energy affecting late time behaviour. When matter density is fixed and curvature is varied, as in Figure 2.3, similar results appear.

In Figure 2.4, dark energy density is held constant and matter density now varies with curvature; $\Omega_M = 1 - \Omega_{DE} - \Omega_K$. This leads to greater expansion velocities at earlier times as opposed to the maximum occuring at $z \sim 1$ when matter density is fixed as before. Though in this case, expansion rates are higher for a closed universe than for an open universe. This is due to the higher matter density in closed universes.

## 2.2 Angular Diameter Distance

The angular diameter distance $d_A(z)$

$$d_A(z) = \begin{cases} \frac{c}{H_0(1+z)} \frac{1}{\sqrt{\Omega_K}} \sinh\left(\sqrt{\Omega_K} \int_0^z \frac{dz'}{E(z')}\right) & \text{for } \Omega_K > 0 \\ \frac{c}{H_0(1+z)} \int_0^z \frac{dz'}{E(z')} & \text{for } \Omega_K = 0 \\ \frac{c}{H_0(1+z)} \frac{1}{\sqrt{-\Omega_K}} \sin\left(\sqrt{-\Omega_K} \int_0^z \frac{dz'}{E(z')}\right) & \text{for } \Omega_K < 0, \end{cases} \tag{2.2}$$

is the primary distance tool used to measure distances to the BAO. As such, how it behaves in curved spacetimes is essential to measuring the changes to the distances measured from angular size of the BAO.

First, in order to conserve the total energy density $\Omega$ at 1, $\Omega_M$ was fixed to be 0.3 and $\Omega_{DE}$ was left to vary with curvature, $\Omega_{DE} = 1 - \Omega_M - \Omega_K$. With $|\Omega_K| = 0.05$, dark energy density then took the values 0.65 in an open universe and 0.75 in a closed universe.

To observe how distance changes between models for a given redshift $z$, $d_A(z)/d_A(z)^{flat}$ is plotted in Figure 2.5, where the values for $d_A(z)^{flat}$ are the fiducial values given in Table 2.1. At low redshifts, $z < 3$, distances in a closed universe are farther than those in a flat universe, with the distances measured in an open universe the shortest. Around $z \sim 3$ the distance measures swap around, with distances in a closed universe now the shortest. The greatest difference between distances measured at low redshifts can be found at $z \sim 1$, on the order of a one percent difference between the distance measured in a curved space and that measured in flat space. As seen in Figure 2.6, which measures the difference from the fiducial model, $d_A(z) - d_A(z)^{flat}$, this amounts to an approximate difference of 15 Mpc between curved space and flat space around $z \sim 1$.

Figure 2.7 displays the changes from a flat model for different matter densities with a fixed curvature density, whilst in Figure 2.8 this is repeated but matter density is fixed and curvature density varies. In both cases dark energy is still left to vary as before. In Figure 2.7, a low density model produces a two percent difference in measured distances, whilst conversely, in Figure 2.8 it is a high curvature density model that displays the greatest difference in distance between spacetime geometries. These results, except for those in Figure 2.6, are the same for the luminosity distance, $d_L$.

The process is now repeated for a fixed $\Omega_{DE}$. Figure 2.9 displays $d_A(z)/d_A(z)^{flat}$ for $\Omega_{DE} = 0.7$ and matter density being left to vary in order to preserve total energy density, $\Omega_M = 1 - \Omega_K - \Omega_{DE}$. In this case, distances in an open universe are uniformly larger than those in a flat universe, with distances in a closed universe the least. In Figure 2.10, $\Omega_{DE}$ is again fixed with the curvature density varying between $|0.01|$ and $|0.09|$. Figure 2.11 displays the case where $\Omega_{DE}$ changes between 0.1 and 0.9, with curvature density fixed at $|0.05|$. These plots, especially Figure 2.11, show that the difference between the distance measured for a given redshift in an open universe and a flat universe is larger than the difference between a flat and a closed universe. At higher redshifts, the divergence between the open model and the flat model is much greater than that between the closed model and the flat model for $\Omega_{DE} = 0.9$. This is caused by the differences in matter density, with the low matter density for the open model resulting in a universe that is almost entirely dominated by dark energy. Such a universe would have expanded much more rapidly than other models, leading to the greater distances measured.

This difference in behaviour between whether $\Omega_{DE}$ or $\Omega_M$ is fixed can be explained

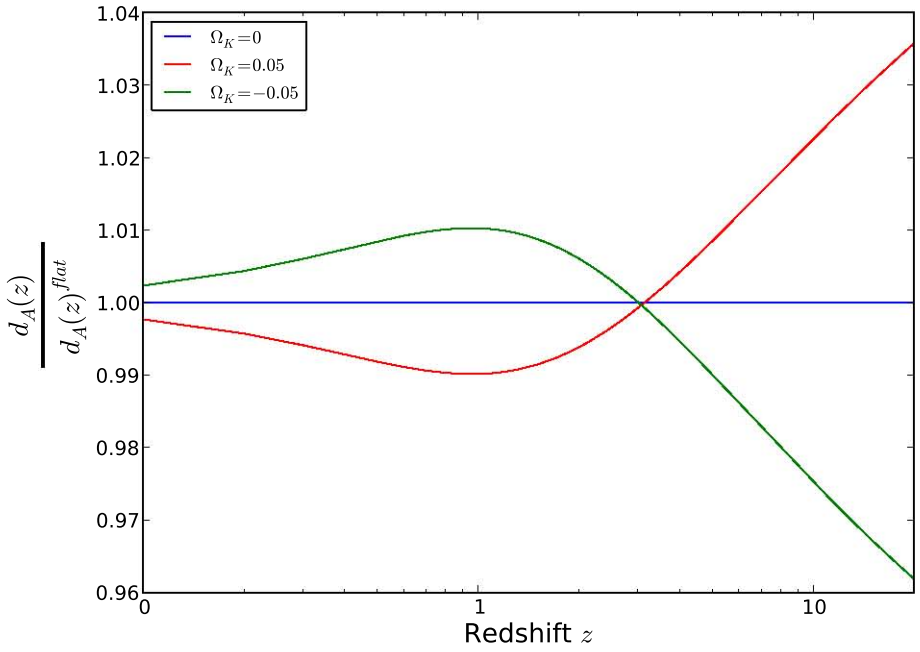


Figure 2.5: Angular diameter distance with $\Omega_M = 0.3$ and $\Omega_{DE}$ left to vary with curvature, $\Omega_{DE} = 1 - \Omega_M - \Omega_K$. Distances in a closed universe are initially higher with distances in the open universe the lowest. Around $z \sim 3$ the models change around.

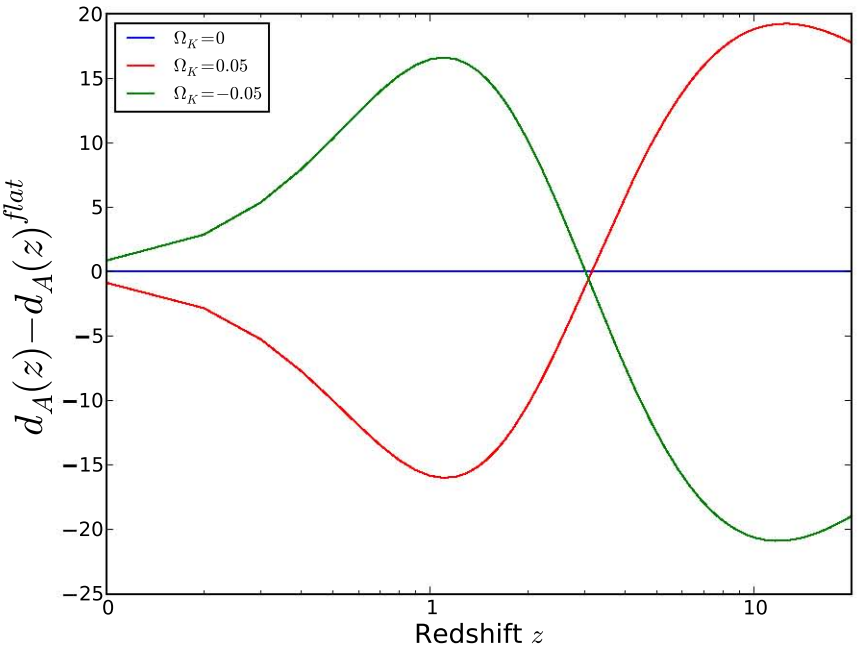


Figure 2.6: The difference between angular diameter distance for curved spaces and flat space with $\Omega_M = 0.3$ and $\Omega_{DE}$ left to vary with curvature. At $z \sim 1$ the difference between the models is approximately 15 Mpc.

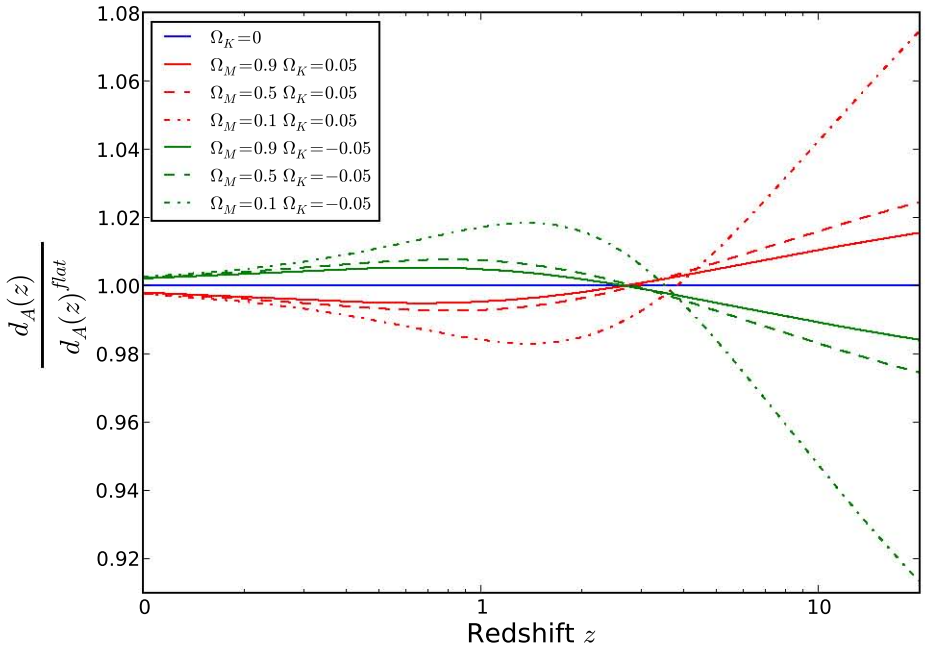


Figure 2.7: The values of $\Omega_M$ vary between a low density model and an almost Einstein-de Sitter universe, with curvature density fixed at $|\Omega_K| = 0.05$. The lowest density models have the greatest divergences from the flat case with the high density models almost resembling the fiducial case at low redshifts.

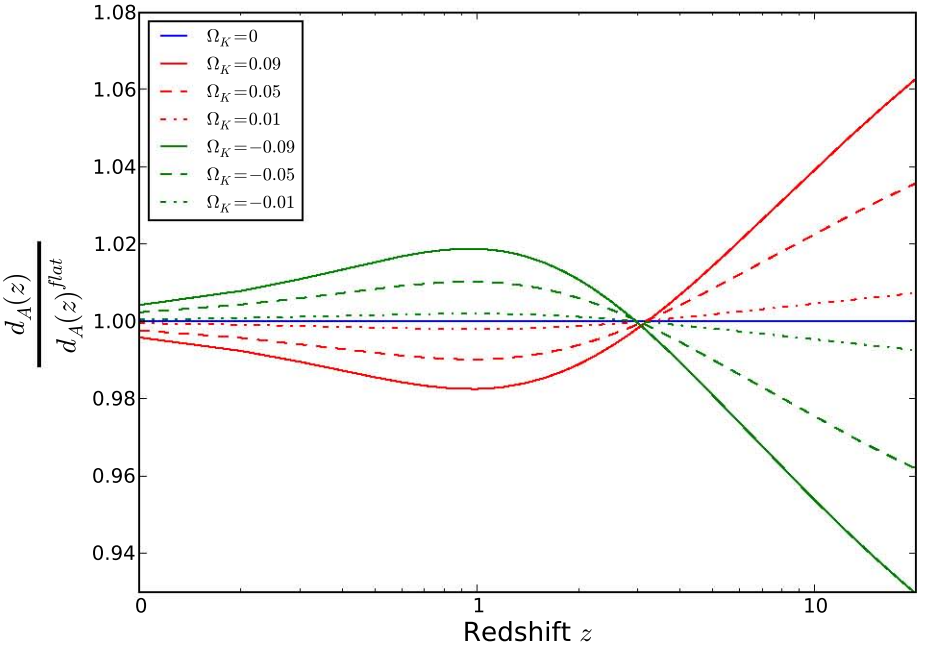


Figure 2.8: Matter is now fixed at $\Omega_M = 0.3$ and $\Omega_K$ is left to vary, with dark energy density correspondingly determined as $\Omega_{DE} = 1 - \Omega_M - \Omega_K$.

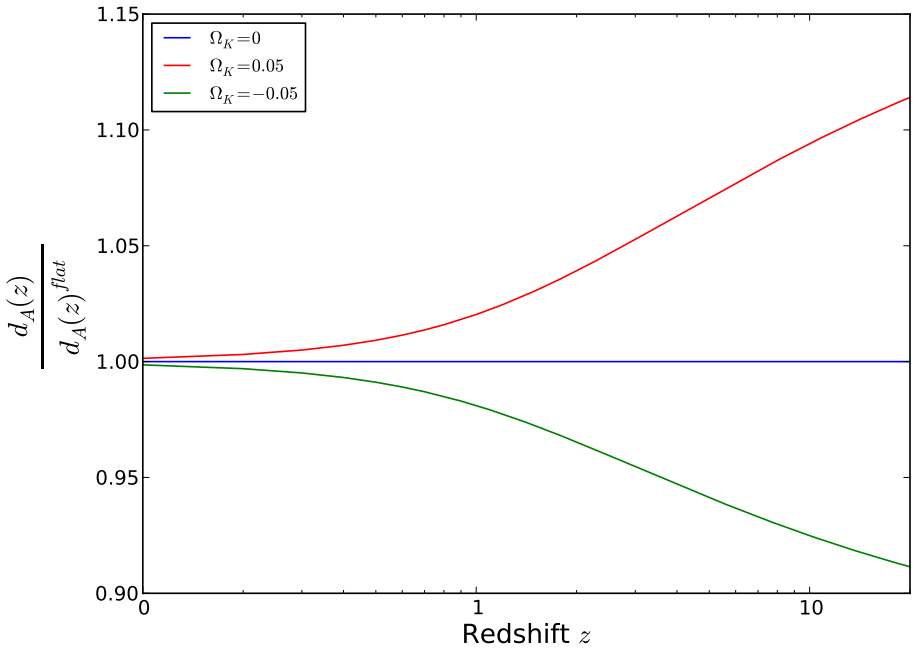


Figure 2.9: Dark energy density is fixed at $\Omega_{DE} = 0.7$ and matter density is left to vary with curvature, $\Omega_M = 1 - \Omega_K - \Omega_{DE}$. Distances in the open universe are the highest for any redshift and the lowest for the closed case.

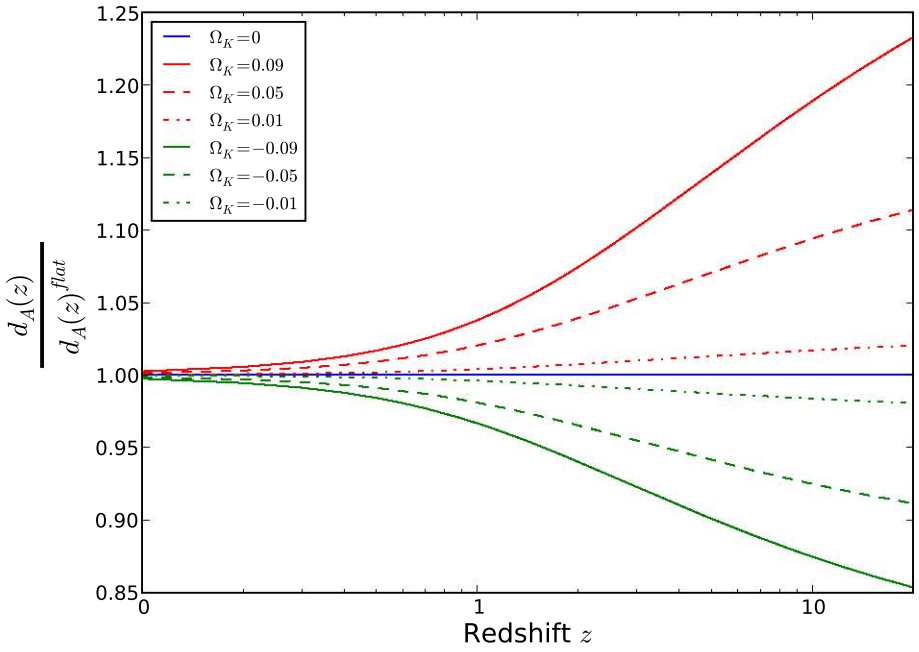


Figure 2.10: A fixed dark energy density, $\Omega_{DE} = 0.7$, with $\Omega_K$ varying between different curvature models and matter density determined by $\Omega_M = 1 - \Omega_{DE} - \Omega_K$

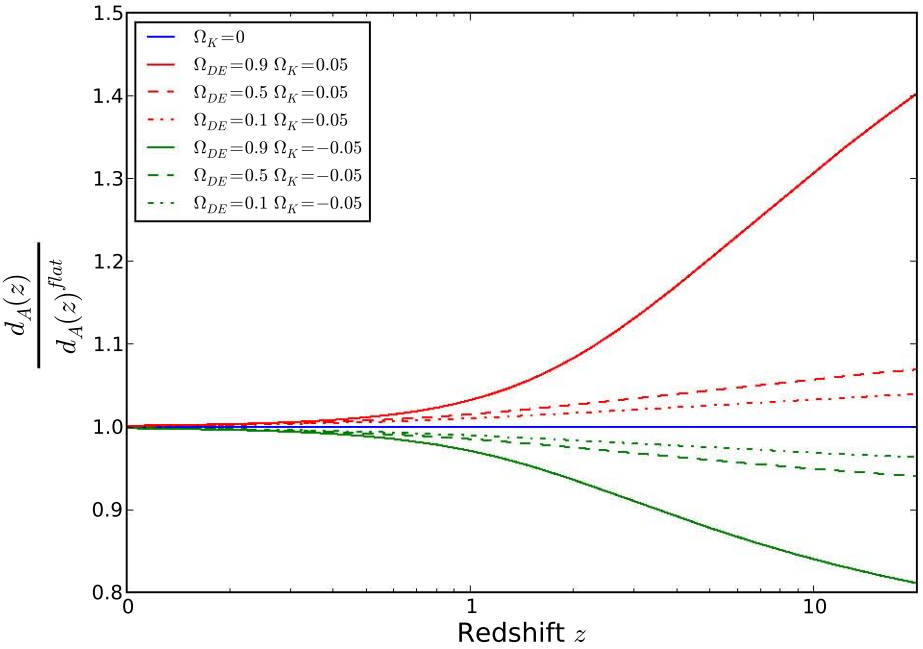


Figure 2.11: In this case, $\Omega_{DE}$ is given different values whilst curvature density is fixed at $\Omega_K = 0.05$. Matter density still varies to preserve the total energy density. The high dark energy content and low matter density in the open universe with $\Omega_{DE} = 0.9$ would cause this model to expand much more rapidly than other models.

by analysing the angular diameter distance equation. Dividing out the Hubble distance $\frac{c}{H_0}$ and Taylor expanding the dimensionless $d_A(z)$ around $z = 0$ gives

$$\begin{aligned} d_A(z) = & \frac{1}{\sqrt{\Omega_M + \Omega_K + \Omega_{DE}}} z \\ & - \left( \frac{1}{\sqrt{\Omega_M + \Omega_K + \Omega_{DE}}} + \frac{3\Omega_M + 2\Omega_K}{4(\Omega_M + \Omega_K + \Omega_{DE})^{3/2}} \right) z^2 + \mathcal{O}(z^3). \end{aligned} \tag{2.3}$$

By definition $\Omega_M + \Omega_K + \Omega_{DE} = 1$, therefore

$$d_A(z) = z - \left( 1 + \frac{3}{4}\Omega_M + \frac{2}{4}\Omega_K \right) z^2 + \mathcal{O}(z^3). \tag{2.4}$$

If instead dark energy is fixed and $\Omega_M$ varies with curvature, then Eq. (2.4) becomes

$$d_A(z) = z - \left( \frac{7}{4} - \frac{3}{4}\Omega_{DE} - \frac{1}{4}\Omega_K \right) z^2 + \mathcal{O}(z^3). \tag{2.5}$$

The first Taylor polynomial dominates at low redshifts $z < 1$, after which the second polynomial controls the behaviour of the function. However, as the first polynomial is the same for both open and closed models, the second polynomial is what determines which distance is greater for a given redshift. For a fixed matter model represented by Eq (2.4), this second term is greater for a closed universe, causing the greater distance measured. For a fixed dark energy model, Eq. (2.5), the converse is true. However, this does not give any insight into why distances in a closed model would become the smaller distances at higher redshifts for a fixed matter density model.

### 2.2.1 Taylor Expansion of Angular Diameter Distance Around $\Omega_K = 0$

The effect of curvature on the measurement of the angular diameter distance can be further studied by Taylor expanding $d_A(z)$ around $\Omega_K = 0$. In order to simplify the calculation, only the dimensionless angular diameter distance is considered;

$$(1+z)\frac{H_0}{c} d_A(z) = \frac{1}{\sqrt{-\Omega_K}} \sin\left( \sqrt{-\Omega_K} \int_0^z \frac{dz'}{E(z')} \right). \tag{2.6}$$

As this is valid for any redshift, $z$ is fixed to be constant. Using the substitution $x = \sqrt{-\Omega_K}$ gives the equation

$$f(x) = \frac{\sin\left(x\, g(x)\right)}{x}, \tag{2.7}$$

where

$$g(x) = \int_0^z \frac{dz'}{E(x, z')}. \tag{2.8}$$

Taking the Taylor expansion of $xf(x) = \sin(x\,g(x))$ around $x = 0$ gives

$$xf(x) = x\,g(x) + \frac{x^3}{3!}(3g''(x) - g(x)^3) + \mathcal{O}(x^5), \tag{2.9}$$

where $' = d/dx$. Therefore

$$f(x) = g(x) + \frac{x^2}{3!}(3g''(x) - g(x)^3) + \mathcal{O}(x^4). \tag{2.10}$$

Calculating $g(x)$ and $g''(x)$ for $x = 0$ requires that $\frac{\partial}{\partial x}\int_0^z \frac{dz'}{E(z',x)} = \int_0^z \frac{\partial}{\partial x}\frac{dz'}{E(z',x)}$. Further, to preserve total energy density $\Omega$ as 1, $\Omega_{DE} = 1 - \Omega_M + x^2$. Resubstituting $x = \sqrt{-\Omega_K}$, $g(0)$ and $g''(0)$, multiplying by $\frac{c}{H_0(1+z)}$ and ignoring higher order terms gives the Taylor expansion of angular diameter distance around $\Omega_K = 0$,

$$d_A(z) = \frac{c}{H_0(1+z)}\left(\int_0^z \frac{dz'}{E_{k=0}(z')} + \frac{\Omega_K}{6}\left(\int_0^z \frac{dz'}{E_{k=0}(z')}\right)^3 + \frac{\Omega_K}{2}\int_0^z \frac{1-(1+z')^2}{E_{k=0}(z')^3}dz'\right); \tag{2.11}$$

where $E_{k=0}(z) = \left(\Omega_M(1+z)^3 + 1 - \Omega_M\right)^{1/2}$. Whilst this was calculated using the angular diameter distance for a closed universe, the result is equally valid for an open universe. The accuracy of these derivations is displayed in Figure 2.12 and Figure 2.13. A full derivation of this result is given in Appendix A.

As seen in Eq. (2.11), the effects of curvature upon the angular diameter distance are due to the presence of the dimensionless radial distance cubed

$$(d_R(z))^3 = \frac{1}{6}\left(\int_0^z \frac{dz'}{E_{k=0}(z')}\right)^3, \tag{2.12}$$

and its derivative

$$\frac{\partial}{\partial\Omega_K}d_R(z) = \frac{1}{2}\int_0^z \frac{1-(1+z')^2}{E_{k=0}(z')^3}dz'. \tag{2.13}$$

These two terms are multiplied by $\Omega_K$ and plotted in Figure 2.14 in order to determine what effect each term has upon the behaviour of $d_A(z)$. As observed in Figure 2.14, the derivative term dominates at low redshifts and the cubed term at higher redshifts. This is the reason for the closed universe having greater distances initially for a fixed matter model.

## 2.3 Distances Between Objects in Redshift Space

Since the BAO are measured from the distances between galaxies in space, an investigation into how these distances change with regards to one another for models of different

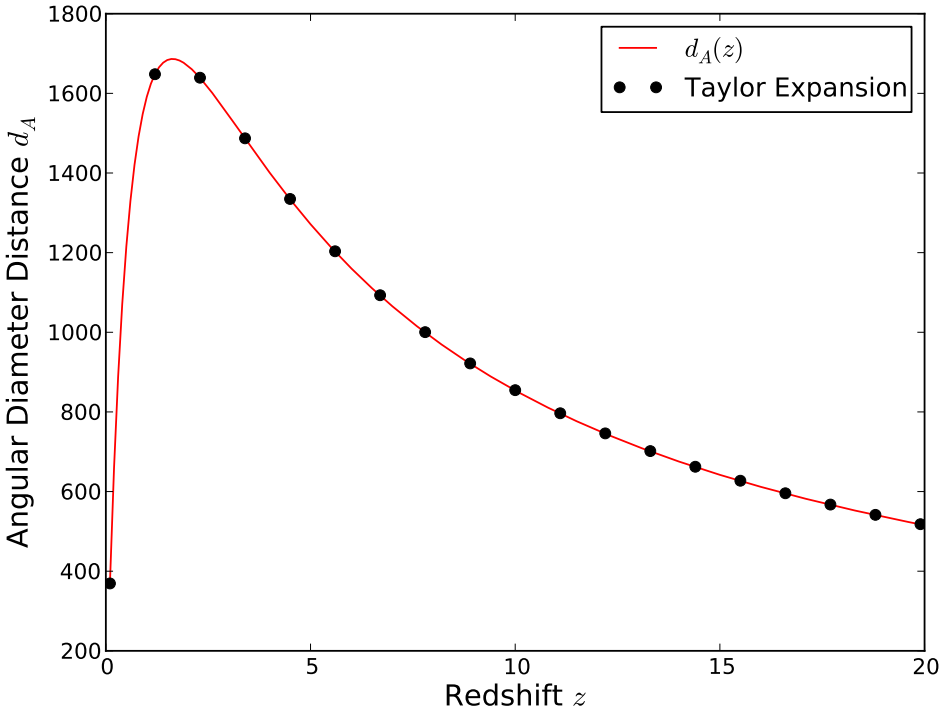


Figure 2.12: The angular diameter distance and its expansion around $\Omega_K = 0.05$ for an open universe.

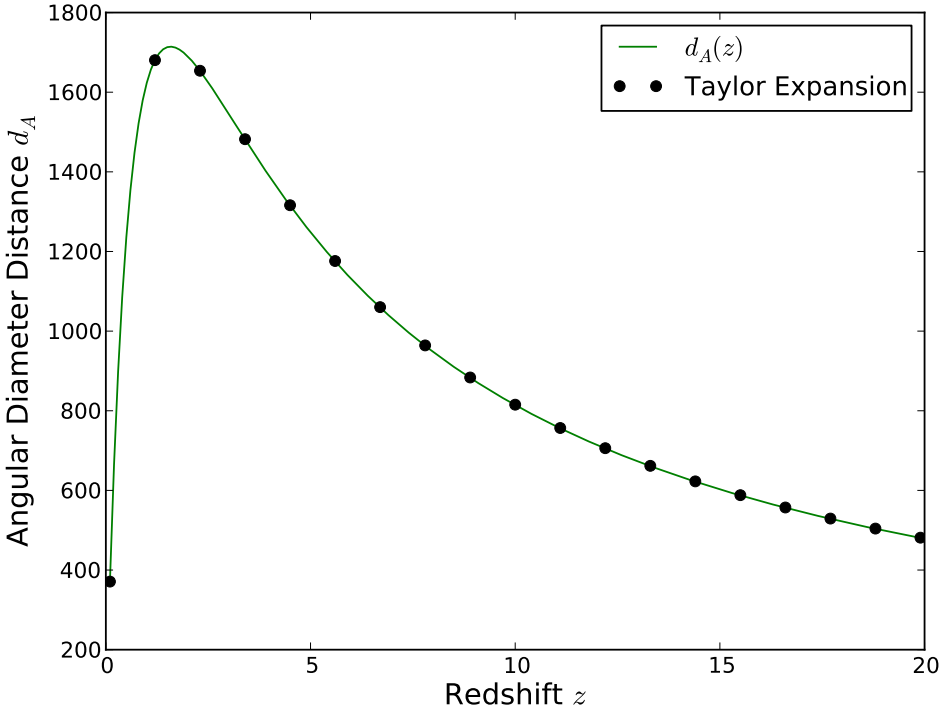


Figure 2.13: The angular diameter distance and its expansion around $\Omega_K = -0.05$ for a closed universe.

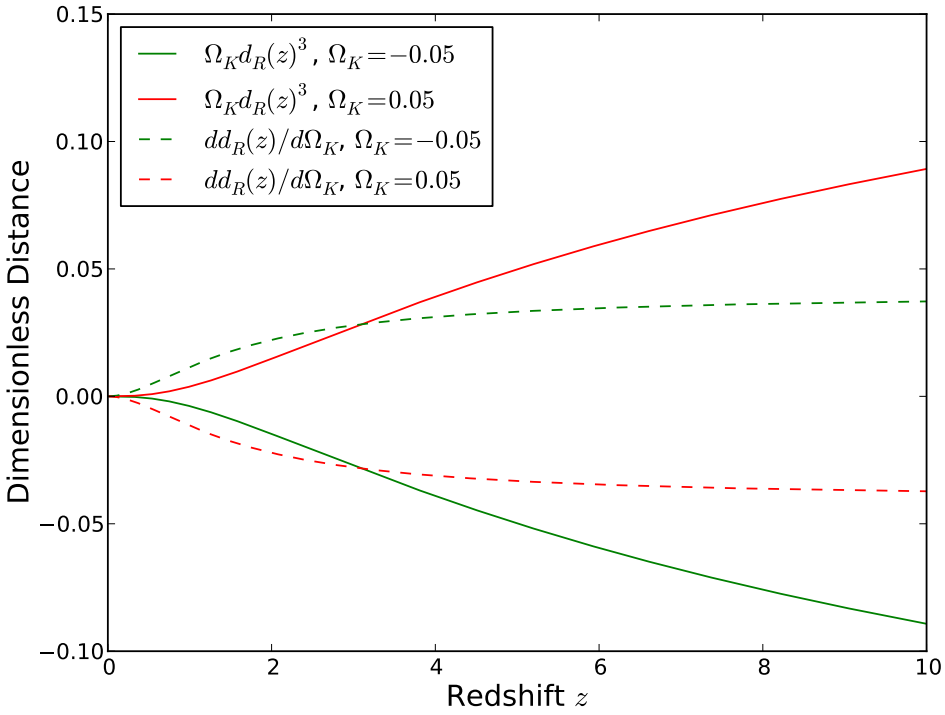


Figure 2.14: The radial distance cubed, Eq. (2.12) and its derivative, Eq. (2.13) from the Taylor expansion for $d_A(z)$, Eq. (2.11). Initially, the derivative term dominates at low redshifts, causing the closed universe to have greater distances. Around $z \sim 3$ the cubed term then dominates, causing the open universe to then have the greater distances.

curvature density is conducted. The comoving seperation between two objects located at $z_1$ and $z_2$ can be calculated from [67]

$$x_{12}^2 = x_1^2 + x_2^2 - kx_1^2x_2^2(1 + \cos^2\theta_{12}) - 2x_1x_2\sqrt{1 - kx_1^2}\sqrt{1 - kx_2^2}\cos\theta_{12}, \tag{2.14}$$

where $k$ the curvature parameter, $\theta_{12}$ is the observed angular seperation and $x_1 = d_A(z_1)$ and $x_2 = d_A(z_2)$ are the angular diameter distances to the two objects.

To investigate just how the distances between objects would vary for models with different curvature densities, two objects were held at a fixed angular seperation of $\theta = 10°$ and at the same redshift as each other. Then the redshifts for both objects were increased at equal rates, with the distance between them measured for different curvature densities. The results are plotted in Figure 2.15a. The difference between the distances measured for the two curved models and the flat model, $\Delta x_{12} = x_{12}^{curved} - x_{12}^{flat}$ is plotted in Figure 2.15b. As expected, for two objects at equivalent redshift and angular seperation, increasing the redshift will increase the distance between them.

When measuring the distances between galaxies in order to calculate the 2-point correlation function, it is rare to find two galaxies at the same redshift; most galaxies are found at different redshifts from each other. To investigate how this would change the distances measured between two galaxies, the same method as before is used, except one galaxy is constantly at a redshift of $z = 0.2$ farther than the other. The results are plotted in Figure 2.16a. The distance measured between the galaxies at different redshifts starts very high regardless of the geometry, and then decreases with increasing redshift to the level recorded in Figure 2.15a at $z = 1$. The reason for this is that distance does not increase linearly with redshift. At very low redshifts, a redshift difference of 0.2 will be much greater than for the same redshift difference at higher redshifts. This is why around redshift $z \sim 1$ the small difference in redshift does not contribute much to the distance measured between two galaxies.

Figure 2.16b is the difference $\Delta x_{12}$. In this case, for higher redshifts, the difference in the distance measured for the different cosmologies is practically constant. This suggests that for objects at different redshifts to each other, changing the cosmology will not drastically change the distance measured between them.

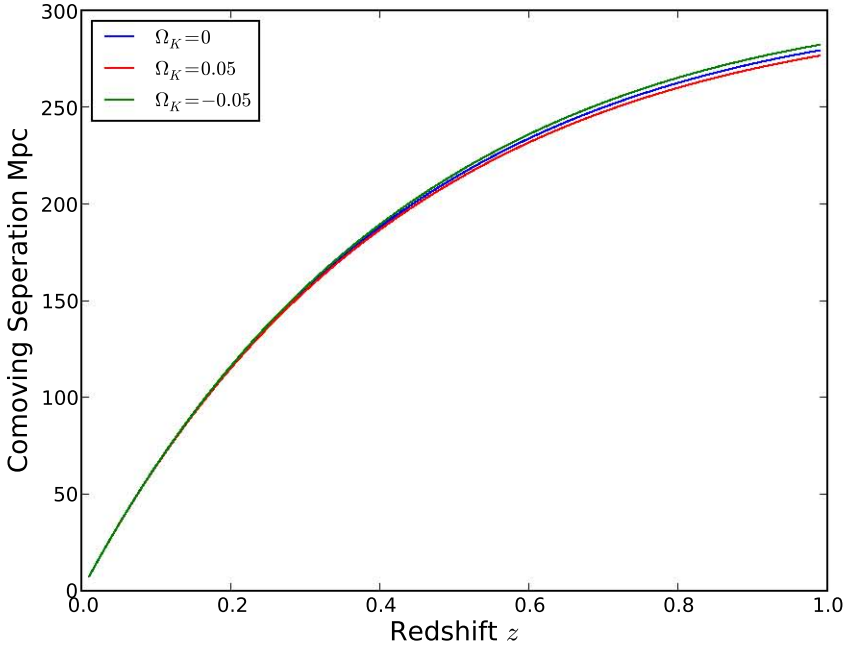


(a) The distance between two objects with an angular seperation of $\theta = 10°$ for open, closed and flat geometry models.

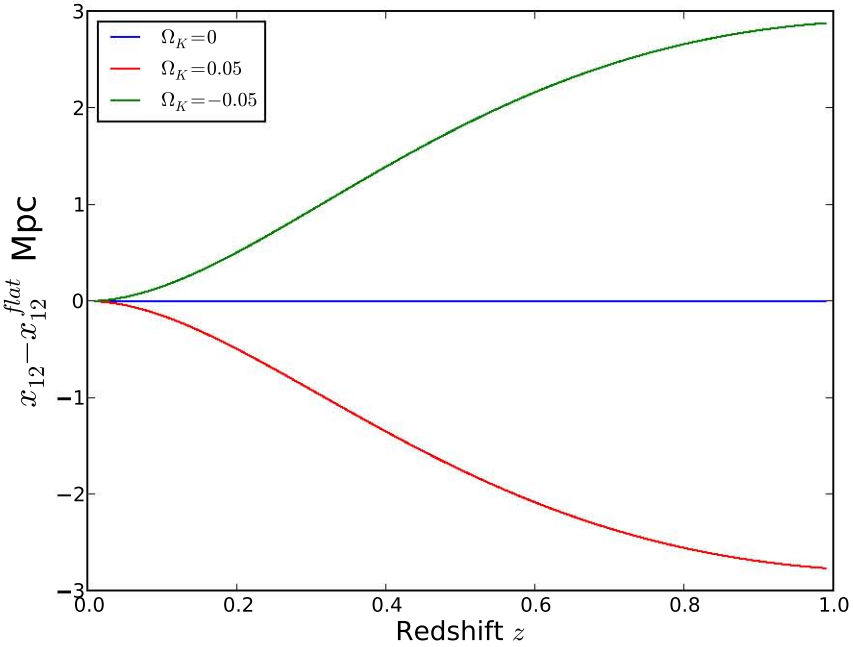


(b) The difference in distance between the curved models and the flat case, with distances at $z \sim 1$ a few Mpc different to the flat model.

Figure 2.15: Two objects are kept at a constant angular seperation of $\theta = 10°$ and are fixed to be at an equivalent redshift. The distance between the objects was then measured for different curvature densities as redshift was increased up to $z = 1$.

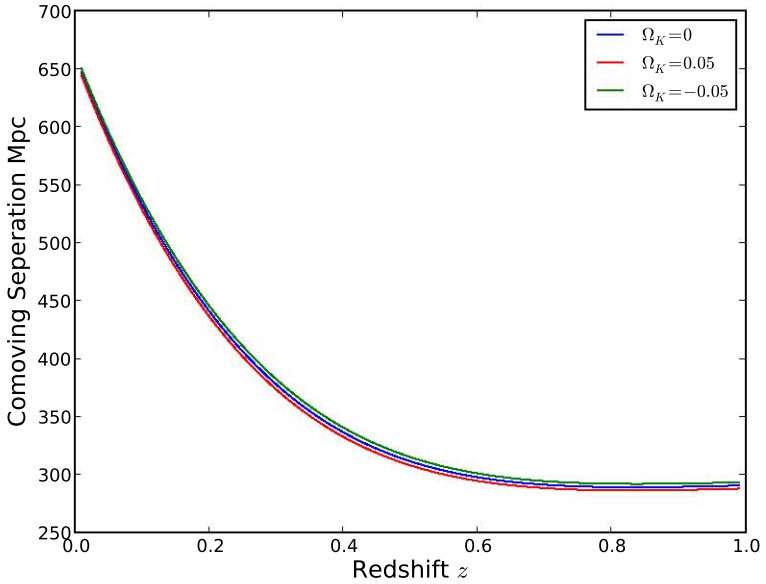


(a) The distance between two objects with an angular seperation of $\theta = 10°$ for open, closed and flat geometry models with the one object constantly at a redshift of 0.2 greater than the other.

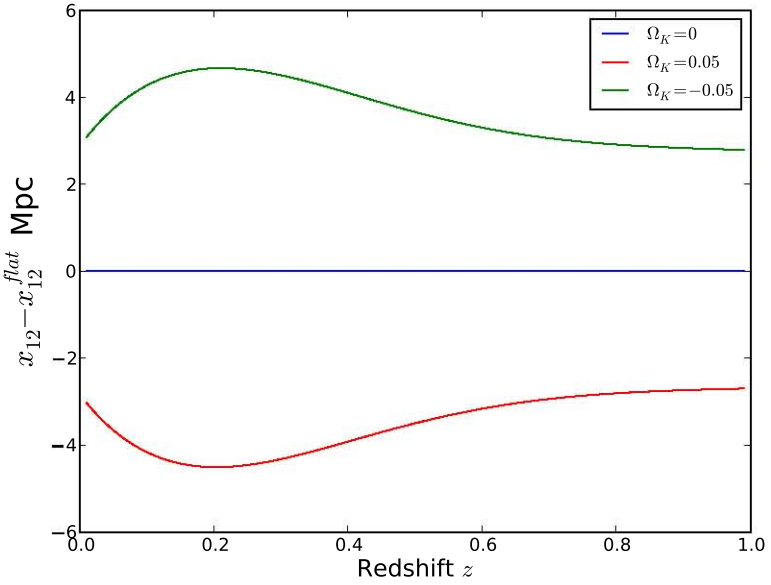


(b) The difference in distance between the curved models and the flat case. In this case, the distance between the curved cases and the flat case looks mostly constant for any redshift.

Figure 2.16: Two objects are kept at a constant angular seperation of $\theta = 10°$, though one object has a redshift of 0.2 greater than the other. The distance between the objects was then measured for different curvature densities as redshift was increased up to $z = 1$.

## 2.4 Conclusion

The Hubble parameter is a measure of the expansion history of the Universe, and the angular diameter distance is the primary method used to determine the distance to objects in redshift space. For a given redshift, different matter and energy contents of the Uuiverse will result in different values being measured for these quantities. Though whether a closed universe will give the farthest distance at low redshifts depends upon whether matter density is fixed and dark energy is left to vary with curvature, with the opposite case resulting in open universes having the greater distances at low redshifts.

Interestingly, the distance measured between objects in redshift space does not change much between open, closed, and flat models; on the order of 2 or 3 Mpc. This suggests that the acoustic scale for the Baryon Acoustic Oscillations will not differ by much when measured with models using different curvature densities. This will be investigated in the next chapter.

# Chapter 3

# The Baryon Acoustic Oscillations in Curved Spacetimes



## 3.1 Introduction

Currently, when the BAO are measured, flatness is assumed when the redshifts of galaxies are converted into distances. Once the 2-point correlation function has been measured and the BAO scale determined, the results are used to constrain cosmological parameters, curvature amongst them. This is a case of assuming flatness to measure how flat the Universe is.

There exists justification that changing the cosmology of the Universe will cause the BAO scale to change accordingly. Seo *et al* considered what would happen to the BAO scale when the fiducial model is changed [68]. When the sum of matter density and dark energy density is not unity, the BAO scale shifts from the concordance ΛCDM model they have taken as their fiducial model.

Further, the BAO scale was measured in simulations containing overdense regions. It was found that in overdense regions the Universe behaves locally like a closed universe, causing the BAO scale to shift to smaller values, $\sim 0.3\%$ less [62]. Added to these are the results from the previous chapter where different values for curvature density will result in different distances being measured for a given redshift. It is conceivable that this will lead to a shift in the BAO scale if an inaccurate cosmology is assumed when calculating the 2-point correlation function.

## 3.2 Method

In order to measure the difference between the 2-point correlation function in a flat universe and in a positively curved closed universe, a 2-dimensional universe was simulated. To create the positive curvature, the universe was simulated on the surface of a sphere; this fulfilled the condition for constant Gaussian curvature which is a property of a homogenous and isotropic universe.

The radius of curvature for a closed universe with $\Omega_K = -0.05$ is calculated using Eq. (1.37);

$$\begin{aligned} R_{curv} &= \frac{H^{-1}}{|\Omega - 1|^{1/2}} \\ &= \frac{3 \times 10^5}{72}(0.05)^{-1/2} \\ &= 18,931\text{Mpc} \end{aligned} \tag{3.1}$$

To represent this, the surface of a sphere of radius 18,931 Mpc is used as the 2-dimensional universe. To create a galaxy catalogue that has a strong correlation signal that can represent the acoustic peak, the following method was used; a space of 2,000 by 2,000 Mpc was subdivided into a grid with a 200 Mpc spacing between grid points. On each of these grid points a point was placed. A ring of points was then placed with this original point in the centre. In order to simulate the nature of the acoustic signal, when each point was placed on the ring, its exact distance was drawn from a normal distribution of mean 151 Mpc and standard deviation 151 Mpc. The number of points in this ring was randomly chosen to lie between 3 and 11. Around each of these points, another ring consisting of a random number of points was placed, also with the same radius. This process was then repeated for these new points. This created a galaxy catalogue that had a large number of galaxy pairs that had a distance of approximately 151 Mpc between them. The reason for the grid system is as follows; initially this process was repeated six times for one initial point. This caused a dense concentration of points in the centre of the distribution and very few on the edges. By instead using many origin points with only a few iterations of points placed around each, a more even distribution of points was created. At this stage, the coordinates for the galaxies are in spherical coordinates, $\theta$ and $\phi$.

An observer was placed 1,000 Mpc from the edge of the galaxy distribution and the distance between this observer and each of the galaxies in the catalogue was measured, with the measurements along the great circle connecting the observer and the chosen

galaxy. This distance was then converted into a redshift using the equation for $d_A(z)$ and $\Omega_K = -0.05$. The angle that the galaxy deviated from the centre of the catalogue space as seen by the observer was also measured. This created a catalogue where the coordinates of all the galaxies were given in redshift and right ascension.

To create the random catalogue, points were placed on the surface of the sphere with the $\theta$ and $\phi$ values chosen as random numbers from within the confines of the survey area. The number of points being placed was determined by how large the galaxy catalogue was, normally on the order of two times more points.

As in an actual correlation measurement, the redshifts and ascension angles were then converted back into a distance and position in the universe using a chosen cosmology to convert from redshift into angular diameter distance. The 2-point correlation function was then measured using Eq. (1.62) in the method outlined below.

Originally, the 2-point correlation was calculated using a grid method; the galaxies were assigned to a grid of 5 by 5 Mpc grid blocks. The distance between different grid points was calculated and weighted according to how many galaxies were in the two grid blocks. This method has the advantage that the amount of time taken to compile is independent of how many galaxies are in the calculation, though this is only an advantage for a large amount of galaxies, more than 30,000 in the data catalogue. But to run with smaller catalogues, it was inefficient, and it was not as accurate as direct point to point correlation measurements. In addition, calculation of the 2-point correlation function in three dimensions is now done for a grid with $n^3$ points. This would be computationally intensive no matter how many data points were in the calculation.

The method that was created is a direct point to point correlation, but to speed up computation times, only galaxies in a specified neighbourhood of the chosen point were included in the calculation. This method was to place all the galaxies, both from the galaxy catalogue and the random catalogue, into a list. The first galaxy in the list was then chosen as the central point in the correlation measurement. Using the coordinates for this galaxy, a region of radius 200 Mpc was created with this galaxy in the centre, and the coordinates of other galaxies were then checked to see if they lay within this region. In this way, only galaxies that were less than 200 Mpc away from the chosen galaxy were included in its correlation measurement. The distance between the centre galaxy and

the chosen galaxies was measured and the results were appropriately binned into either data-data, data-random or random-random bins. The centre galaxy was then removed from the list so that its measurements would not be repeated when one of its companion galaxies was chosen, and the process was repeated with the next galaxy in the list until all the galaxies had been cycled through. A graphical representation of this process is presented in Figure 3.1, with the Python script attached in Appendix B. The 2-point correlation function $\zeta(r)$ was then calculated using a modified version of Eq. (1.62) [69],

$$\zeta(r) = 1 + \left(\frac{N_R}{N_D}\right)^2 \frac{DD(r)}{RR(r)} - 2\frac{N_R}{N_D}\frac{DR(r)}{RR(r)}. \tag{3.2}$$

$N_R$ and $N_D$ are the number of data points in the random catalogue and the galaxy catalogue respectively.

In order to test the robustness of this method, it was used on the galaxy and random catalogue [70, 71, 72] that was used in the original detection of the BAO peak in 2005 by Eisenstein *et al* [26]. This is a galaxy catalogue of 46,748 luminous red galaxies. The result of measuring the 2-point correlation function is presented in Figure 3.2. The results from Eisenstein *et al* are presented in Figure 3.3 for comparison. The results calculated from the above described method are comparable with the original detection, and thus the method used to measure the 2-point correlation function is a valid one.



## 3.3 Results

### 3.3.1 The Shift of the Acoustic Peak

In order to determine if there is a change in the acoustic scale of the BAO peak if an inaccurate cosmology is used, the following steps were done. A data catalogue of 11,896 points was created as described in Section 3.2 where every point was placed approximately 151 Mpc from its origin point on the surface of a sphere of radius 18,931 Mpc. The distribution of these points is represented in Figure 3.4. The distances were converted to redshifts using the cosmology of a closed universe with $\Omega_K = -0.05$. These redshifts, of the order $z \sim 0.3$ to 0.35, were then converted back into angular diameter distances assuming a flat universe, and the 2-point correlation function was measured as described in Section 3.2, using a random catalogue of 20,000 points. As a comparison, the 2-point correlation function was also measured with the original cosmology. The results are plotted in Figure (3.5a) for the original cosmology and in Figure (3.5b) for the flat case.

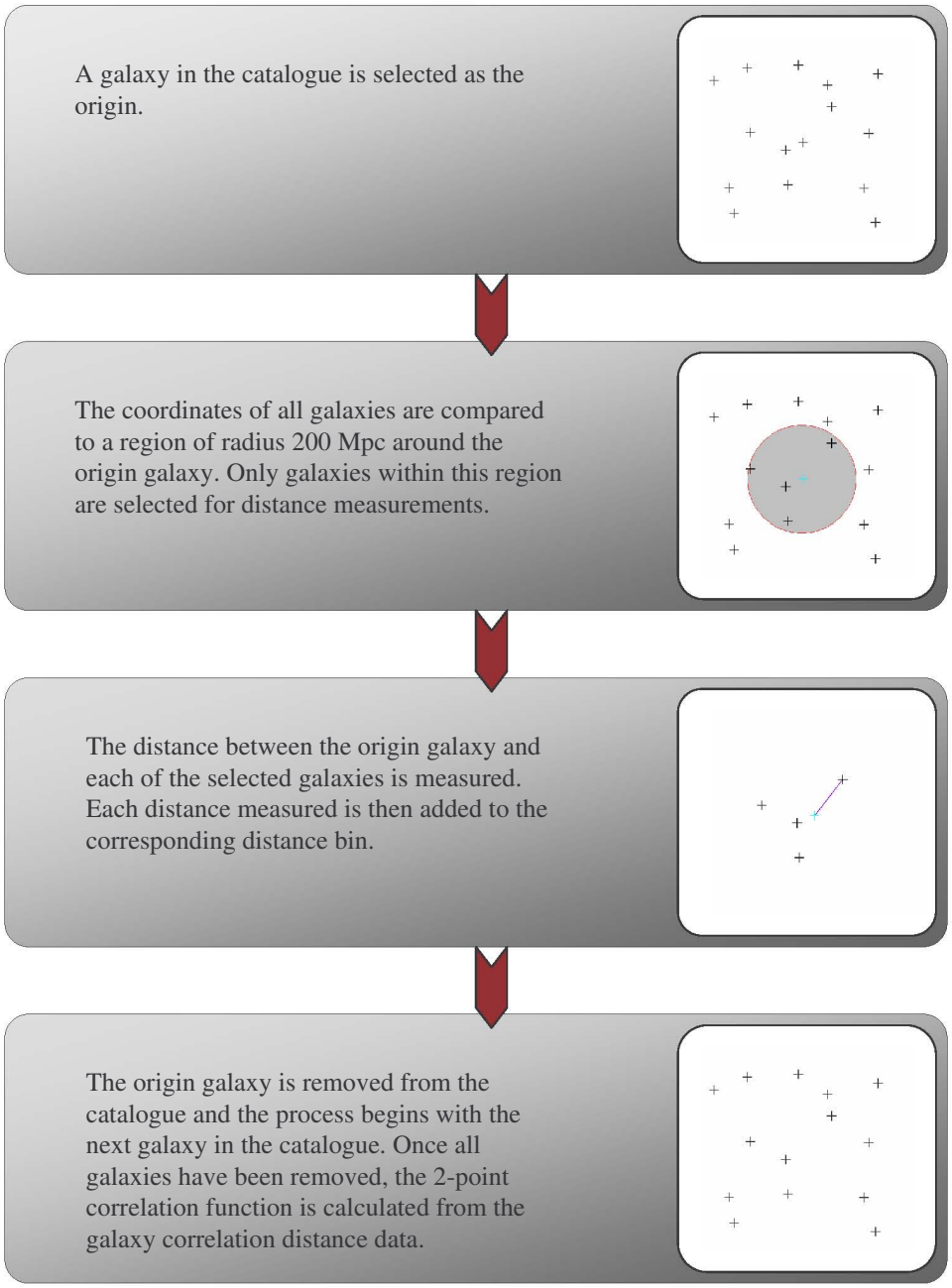


Figure 3.1: A flowchart graphically detailing the steps followed to efficiently measure the number of galaxy pair distance correlations. A copy of the Python script for this process is attached in Appendix B.

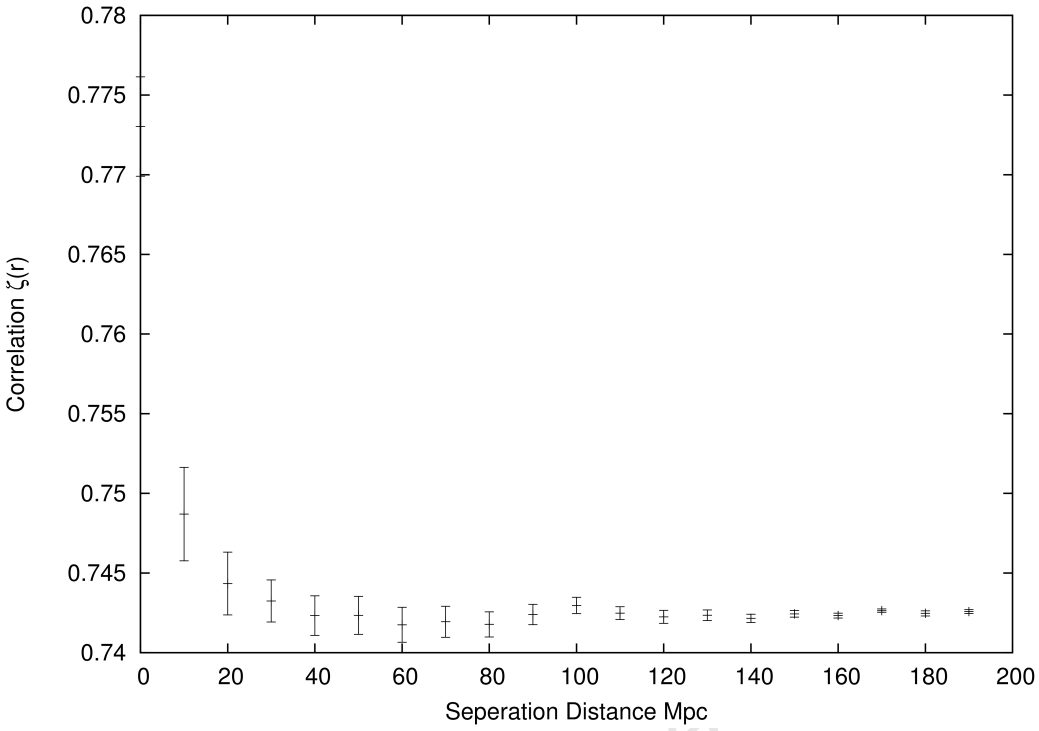


Figure 3.2: The 2-point correlation function for the SDSS DR3 catalogue.

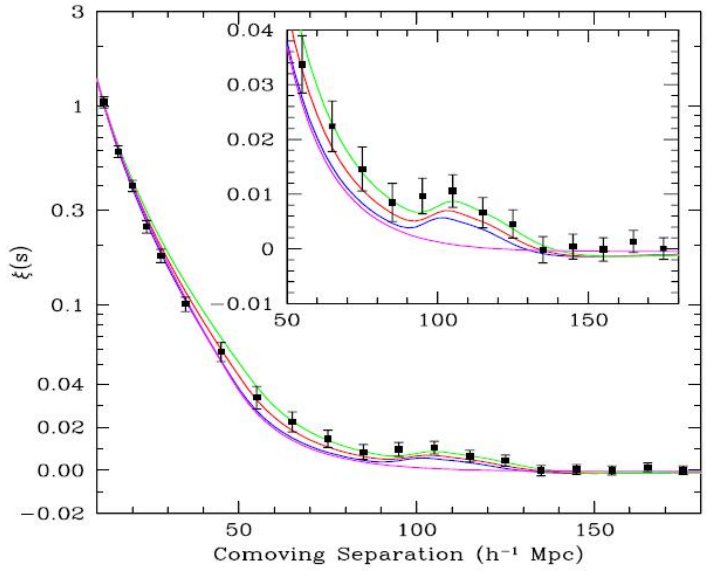


Figure 3.3: The BAO peak as detected by Eisenstein *et al* in 2005. The models are $\Omega_M h^2 = 0.12$ (green), $\Omega_M h^2 = 0.13$ (red), and $\Omega_M h^2 = 0.14$ (blue). The magenta line is for a pure CDM model, $\Omega_M h^2 = 0.105$. Figure taken from [26].

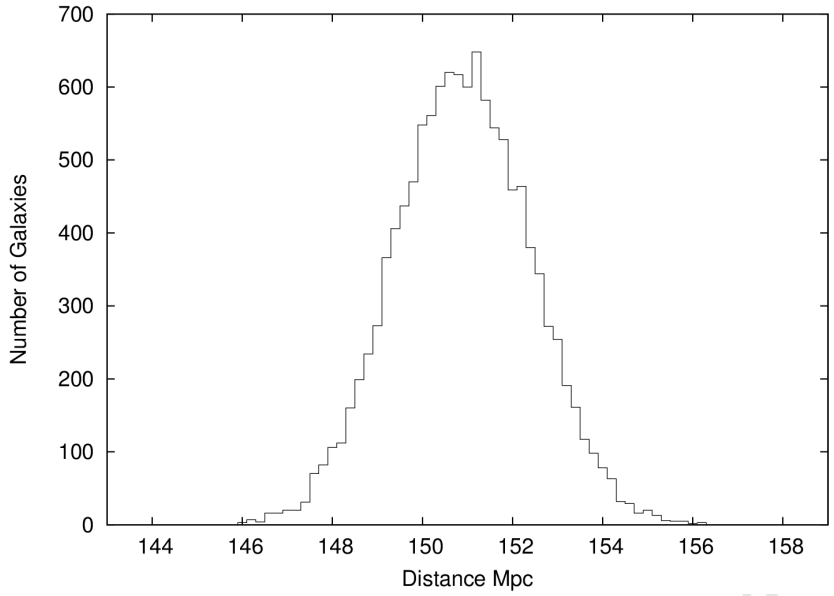


Figure 3.4: The distribution of points chosen for the galaxy catalogue with a mean of 151 Mpc and a standard deviation of 1.5 Mpc.

The error bars are estimated from

$$\text{error}(r) = \frac{1}{\sqrt{DD(r)}}\zeta(r) \tag{3.3}$$

with $DD(r)$ the data-data correlation measurement. From these results, it is observed that the peak has shifted when flatness is assumed. Fitting the peaks with a Gaussian gives the position and the standard deviation; $151.1 \pm 1.9$ Mpc for the original curved universe, which is shifted to $149.8 \pm 1.9$ Mpc for the flat case.

A note on the size of the catalogues; one of the concerns when using a galaxy survey to measure statistical features such as the 2-point correlation function is the shot noise. Too few points will lead to a high error when trying to compute correlations within the galaxy distribution. To accurately calculate the BAO signal from astronomical data, the observers had to wait for surveys to measure a large enough volume of the sky to obtain the 46,000 galaxies that were used to do the correlation measurement. However, in this Universe, the excess of galaxies at a scale of 150 Mpc is approximately one extra galaxy than would normally be expected. This required a very large number of points to measure the acoustic signal. This investigation however, has created mock galaxy catalogues with a very high correlation at 150 Mpc; on the order of 6 extra galaxies. Thus fewer data points are needed to compute the correlation function. Initially, a mock galaxy catalogue of 50,000 data points and a random catalogue of 100,000 was used; the results were no

different to what has been displayed so far. Therefore, the smaller number of points was used to reduce computation time.

Since the results of Section 2.2 indicate that the greatest divergence between distances measured in a closed universe and those measured in a flat universe for the same redshift occur at $z \sim 1$, the above process is repeated with the observer placed at a redshift of 1 from the region containing the galaxy distribution. The results are plotted in Figure 3.6a for the original closed cosmology and in Figure 3.6b for the assumption of flatness.

Surprisingly, the change in the acoustic scale is almost the same as for the lower redshifts, a shift from $153.0 \pm 2.2$ Mpc to $151.5 \pm 1.5$ Mpc. Taking into account the results of Section 2.3 explains why the greater difference in distances up to $z = 1$ does not result in a greater divergence between the location of the acoustic peak in different cosmologies. It was demonstrated that the difference between the distance measured between two galaxies in different cosmologies was of the order of 3 Mpc. Further, this difference was largely independent of redshift, with the divergence being approximately 2 Mpc between lower and higher redshifts. Calculating the difference between the positions of the fitted peaks produces a shift of 1.3 for $z \sim 0.3$ and 1.5 for $z \sim 1$, as displayed in Figure 3.7. Therefore, the shift in the position of the acoustic peak in the event of using the wrong cosmology to measure the 2-point correlation function is dependent entirely upon the distances measured between the galaxies, and not upon the inaccurate distances that are measured between the observer and the galaxies.

In most cases, the 2-point correlation function is positive, yet in the results presented here, it is negative. This is due to how the mock catalogues were created as opposed to the distribution of galaxies in the Universe. In the Universe, galaxies were distributed as described in Figure 1.8; this results in a positive correlation function as demonstrated in Figure 3.2. The mock catalogue lacks this correlation at shorter distances. This results in the $2DR(r)$ term from Eq. (3.2) being much larger than the $DD(r)$ term at all seperation distances, causing the negative result.

In the case of the Unviverse with a curvature density in the region measured by WMAP, $-0.0178 < \Omega_K < 0.0063$, it is expected that the shift would be much smaller. Currently, the uncertainty on the redshift of an object is 3%, if measured photometrically [17]. This causes uncertainty in the measurement of the BAO peak, of around 1%. This

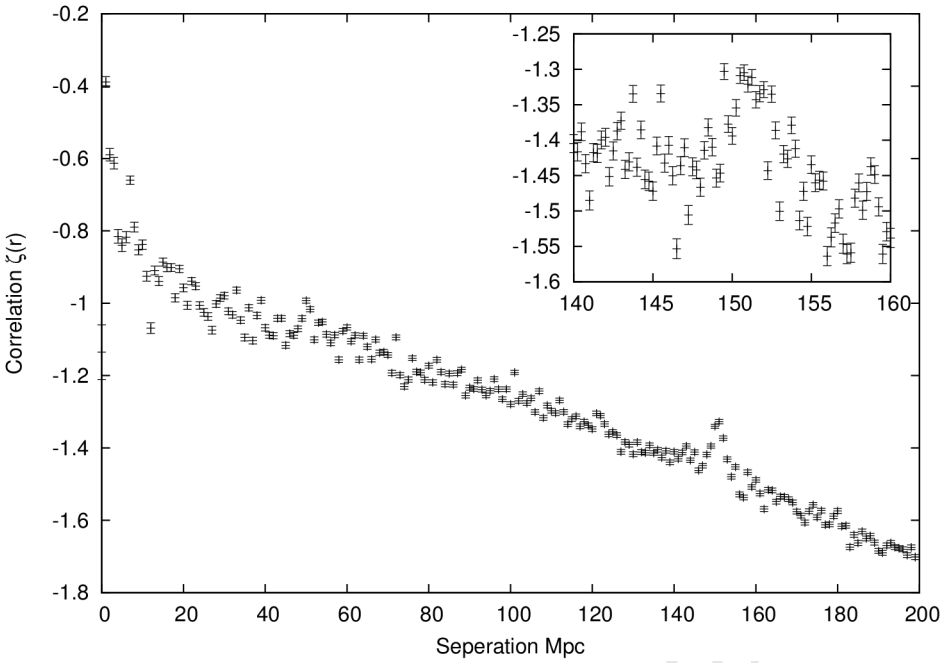


(a) The 2-point correlation function for a universe with $\Omega_K = -0.05$.

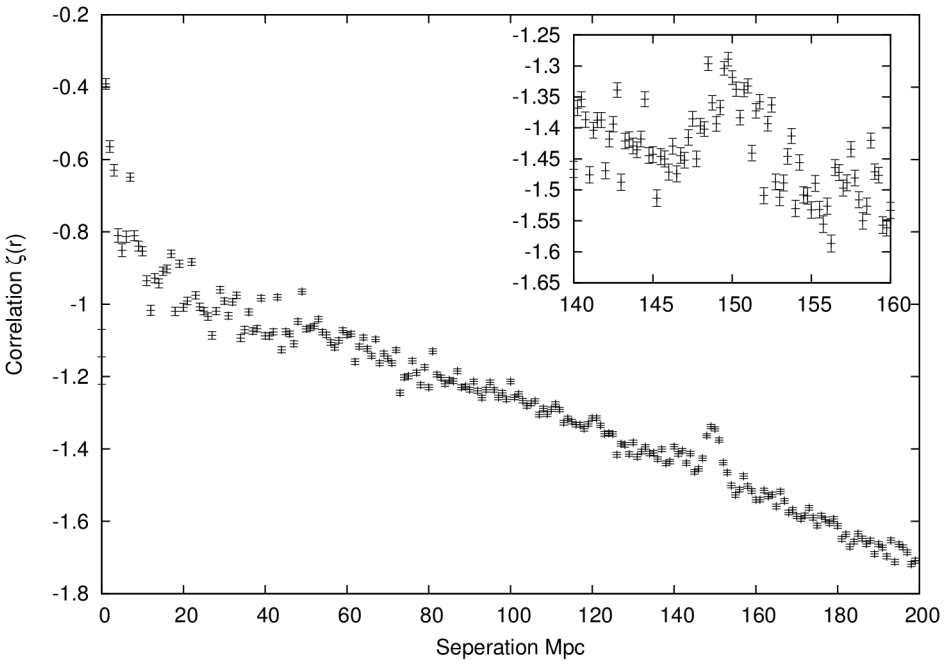


(b) The 2-point correlation function as measured when flatness is assumed.

Figure 3.5: The 2-point correlation function as measured for both a flat universe and a universe with $\Omega_K = -0.05$ for galaxies in the region $z \sim 0.3 - 0.35$. The correlation measurements are in 1 Mpc bins, with the inset figures covering the range of 140 - 160 Mpc in 0.25 Mpc bins. After fitting, the peak for the curved case is at $151.1 \pm 1.9$ Mpc and which is shifted to $149.8 \pm 1.9$ Mpc when flatness is assumed.

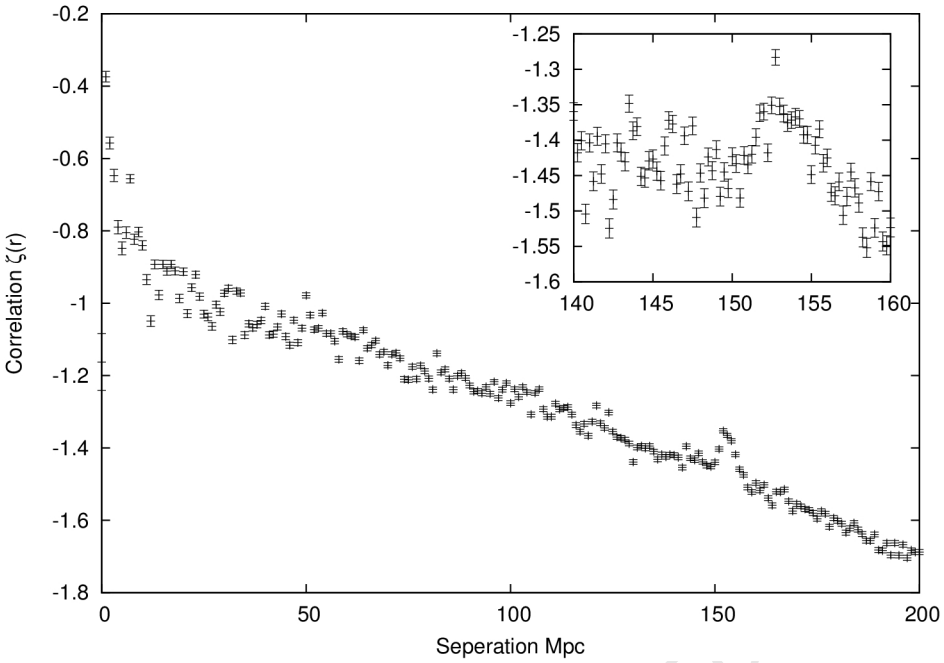


(a) The 2-point correlation function for a universe with $\Omega_K = -0.05$.

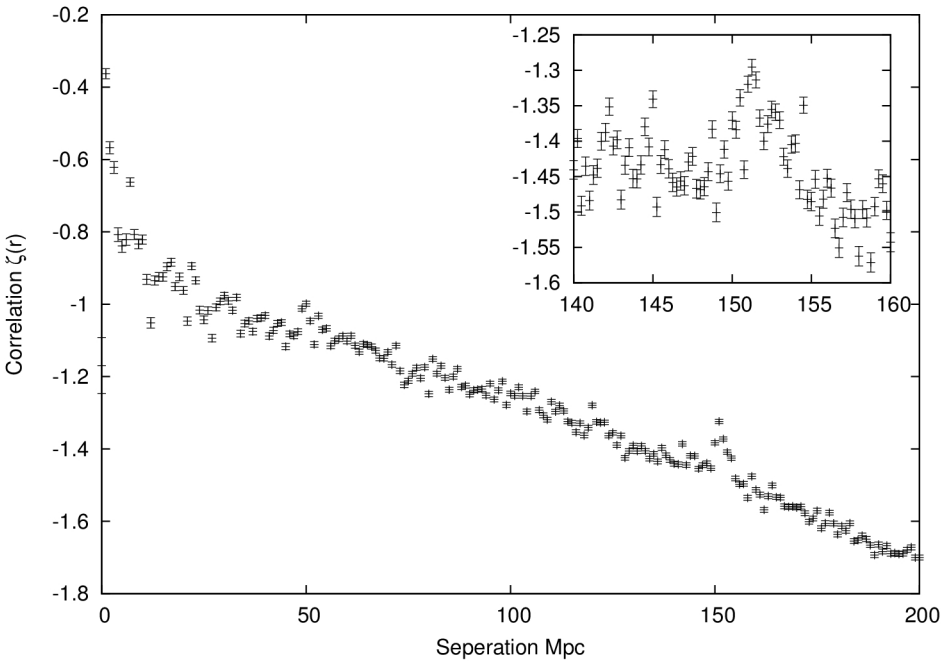


(b) The 2-point correlation function as measured when flatness is assumed.

Figure 3.6: The 2-point correlation function as measured for both a flat universe and a universe with $\Omega_K = -0.05$ for galaxies in the region $z \sim 1.0 - 1.1$. The correlation measurements are in 1 Mpc bins, with the inset figures covering the range of 140 - 160 Mpc in 0.25 Mpc bins. As is observed, the peak has shifted from $153.0 \pm 2.2$ Mpc to $151.5 \pm 1.5$ Mpc when flatness is assumed.

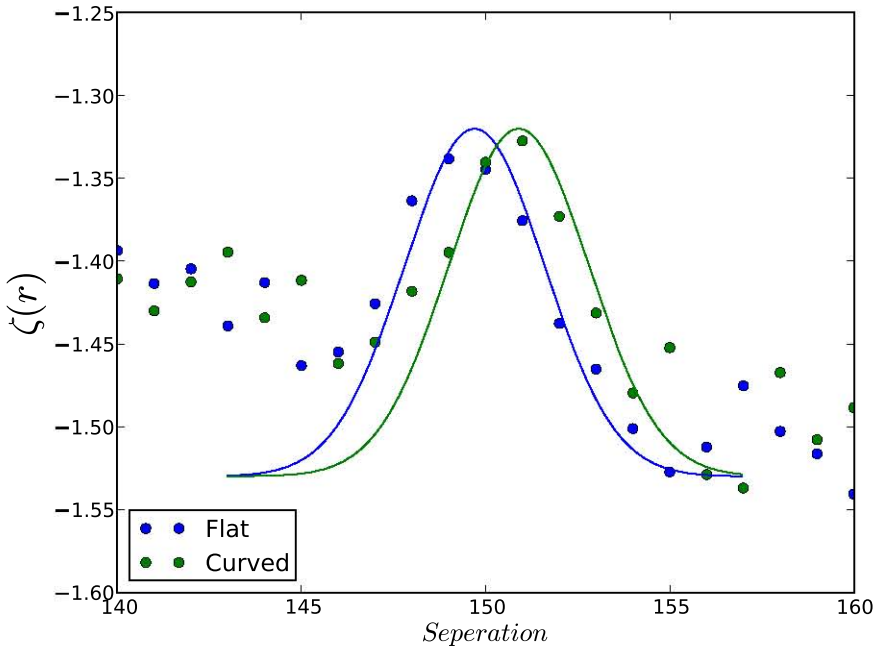


(a) The 2-point correlation function as measured at $z \sim 0.3 - 0.35$.

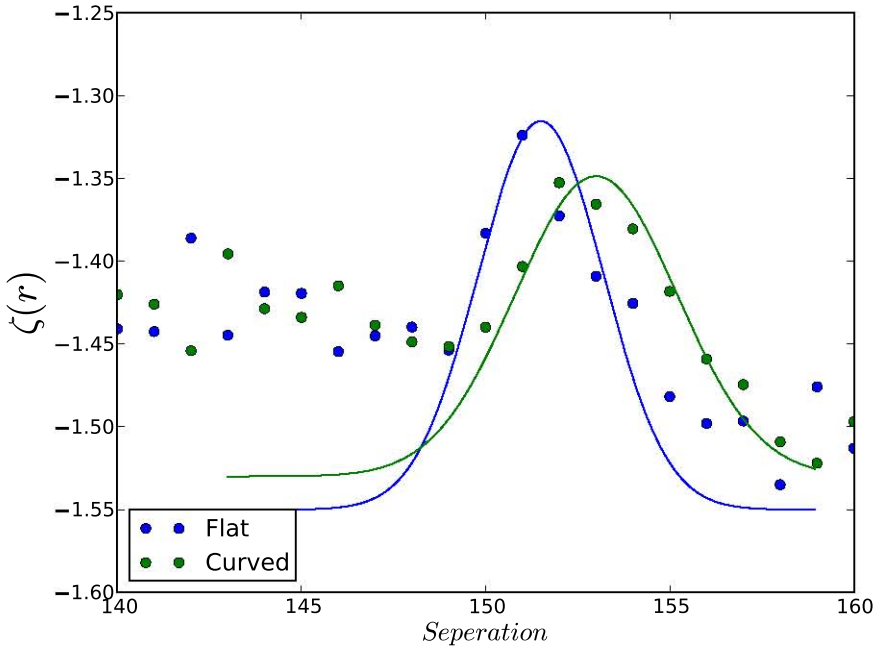


(b) The 2-point correlation function as measured at $z \sim 1$.

Figure 3.7: A comparison of the results of the 2-point correlation function as measured in both cosmological models for the seperation range 140 - 160 Mpc. At redshift $z \sim 0.3 - 0.35$ the difference in the location of the acoustic signal is 1.3 and the difference is 1.5 for $z \sim 1$.

error is in the radial direction only, and so accounts for error in the measurement of the Hubble parameter. Non-linear effects have been demonstrated to provide sub-percent errors on the measurement of the BAO peak [24, 35], though reconstruction has been demonstrated to remove them [59]. This also includes the effect of overdense regions behaving locally like a curved universe causing the BAO peak to shift to shorter distances being removed by reconstruction [62]. Given that the BigBOSS survey intends to measure the BAO peak to sub-percent accuracy [64, 65], it is conceivable that the sub-percent errors caused by assuming the wrong cosmology will adversely affect the measurement of the Hubble parameter and the matter content of the Universe.

Only the closed universe was considered. Due to the complexities of using a surface with hyperbolic geometry to do the same calculations, and given that all distances measured for an open cosmology had the same deviations from flatness as the closed case, the correlation function is not investigated for an open universe; though assuming flatness for an open universe should cause the peak to be measured at a larger distance.

### 3.3.2 The Random Catalogue

In order for the acoustic signal to be determined from the correlation function, the random catalogue should have no correlations or preferred scales within it. This can be checked by a simple calculation; for any point in the random catalogue, the number of correlations expected at a distance can be calculated by comparing the number density to an annulus of radius $dR$ around the chosen point. The calculation is

$$\begin{aligned} dA &= 2\pi \left[(R+dR)^2 - R^2\right] \\ &= 2\pi \left[R^2 + 2R\,dR + dR^2 - R^2\right] \\ &= 2\pi \left[2R\,dR + dR^2\right] \end{aligned} \tag{3.4}$$

Ignoring $dR^2$ as it will be negligible, this results in the straight line $2R\,dR$. As can be seen in Figure 3.8, this is what is returned from the random-random correlation. In this case, the line is not exactly straight but bends towards the $x$-axis slightly; this is due to it being created on the surface of a sphere.

## 3.4 Conclusion

The Baryon Acoustic Oscillations offer a robust distance measure that is based on linear physics. However, assuming an inaccurate cosmology when measuring the position

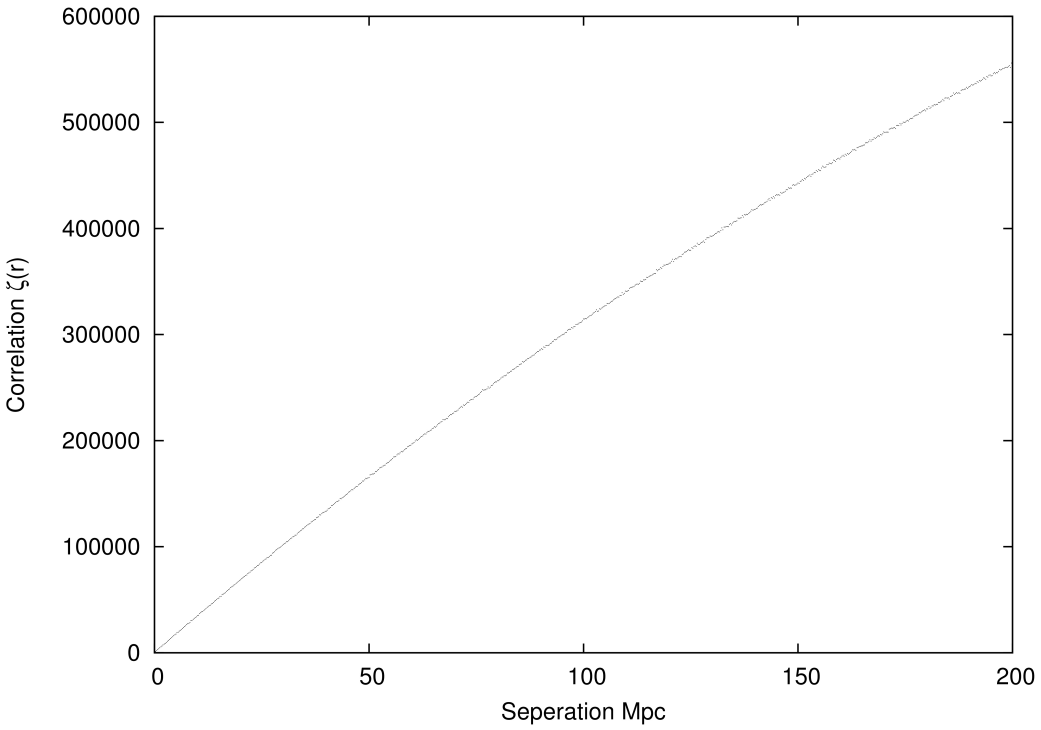


Figure 3.8: The random-random correlation measurement displaying a straight line as calculated in Eq. (3.4)



of the galaxies used to determine the position of the BAO peak will cause an error in the detected signal. Current methods of measuring the acoustic signal involve assuming flatness to measure galaxy positions from survey catalogues. As was displayed in this section, assuming flatness when the actual cosmology was that of a closed universe led to the acoustic signal shifting from $151.1 \pm 1.9$ Mpc to $149.8 \pm 1.9$ Mpc.

The nature of the shift did not depend upon the distances measured between the observer and the galaxies, but instead upon the small difference in the distance measured between galaxy pairs for different cosmologies. This resulted in the shift of the acoustic peak due to a wrong assumption of cosmology to be largely independent of redshift. As the acoustic scale is used as a distance measure, the wrong cosmology will create a larger effect on the distance measured from the BAO scale, than that caused by the small difference in the acoustic scale. This is due to the differences between angular diameter distance measurements done with different cosmologies diverging at higher redshifts.

# Chapter 4

# Conclusion

The Baryon Acoustic Oscillations offer a method to do precision cosmology based on linear physics. From the BAO, distances and the expansion history of the Universe can be accurately measured. This is then used to constrain dark energy and the matter content of the Universe. However, by assuming an inaccurate cosmology when measuring the BAO scale, inaccurate values will be measured for these parameters. Currently, the Universe is assumed to be flat when measuring the BAO scale. It has been demonstrated that an inaccurate assumption of curvature will lead to the acoustic signal shifting from $151.1 \pm 1.9$ Mpc to $149.8 \pm 1.9$ Mpc. Whilst this error in the acoustic scale will remain constant independent of redshift, distance measures and the expansion history will be adversely affected. This is because the shift in the position of the acoustic peak in the event of using the wrong cosmology is dependent entirely upon the distances measured between the galaxies, and not upon the inaccurate distances that are measured between the observer and the galaxies.

Future surveys such as WiggleZ and BigBoss are planning on surveying up to $z \sim 1$ and beyond. Further, the Lyman-$\alpha$ forest and quasars at $z \sim 2$ to 3 can be used to measure the BAO scale for these redshifts. Assuming the wrong cosmology at these distances will lead to small errors in constraining the parameters of the Universe. Presently, curvature is constrained to be $-0.0178 < \Omega_K < 0.0063$ from WMAP measurements combined with BAO and SN Ia data [27]. Since these next generation surveys intend to measure the BAO signal to sub-percent accuracy, the small percentage difference in the curvature density will lead to an inaccurate measurement. To counteract this possibility, model independent measures of the BAO scale, such as that described in [63], can be used to corraborate the results found from methods where an initial cosmology is assumed.

# Bibliography


[1] Aurelius, M., *Meditations*, Penguin Books Ltd, 2006

[2] Haugan, M. P., Lämmerzahl, C., Lecture Notes in Physics, **562**: 195-212 (2001)

[3] Carroll, S. M., arXiv:gr-qc/9712019 (1997)

[4] Weinberg, S., *Gravitation and Cosmology: Principles and Applications of the General Theory of Relativity*, John Wiley & Sons, 1972

[5] *http://www.zamandayolculuk.com/cetinbal/htmldosya1/LightRelavity.htm*

[6] Wald, R. M., *General Relativity*, University of Chicago Press, 1984

[7] Robertson, H. P., The Astrophys Journal, **82**: 284 (1935)

[8] A. G. Walker, Proceedings of the London Mathematical Society **42**: 90 (1936)

[9] Weinberg, S., *Cosmology*, Oxford University Press, 2008

[10] Dodelson, S., *Modern Cosmology*, Academic Press, 2003

[11] Peter, P., Uzan, J. P., *Primordial Cosmology*, Oxford University Press, 2009

[12] *http://map.gsfc.nasa.gov/universe/uni_shape.html*

[13] Kolb, E. W., Turner, M. S., *The Early Universe*, Addison-Wesley Publishing Company, 1990

[14] Riess, A. G., Filippenko, A. V., Challis, P. *et al*, The Astronomical Journal, **116**: 1009-1038 (1998)

[15] Perlmutter, S., Aldering, G., Goldhaber, G. *et al*, The Astrophysical Journal, **517**: 565-586 (1999)

[16] Hogg, D. W., arXiv:astro-ph/9905116 (1999)

[17] Bassett, B. A., Hlozek, R., *Dark Energy* Ed. P. Ruiz-Lapuente, Cambridge University Press, 2010, arXiv: 0910.5224

[18] Blake, C., Parkinson, D., Bassett, B., *et al*, Monthly Notices of the Royal Astronomical Society, **365**: 255-264 (2006)

[19] *http://www.sdss3.org*

[20] Eisenstein, D. J., Weinberg, D. H., Agol, E., *et al*, The Astronomical Journal, **142**: 72 (2011)

[21] *http://www.cosmology.lbl.gov/BOSS*

[22] Eisenstein, D. J., Seo, H.-J., White, M., The Astrophysical Journal, **664**: 660-674 (2007)

[23] Eisenstein, D. J., Hu, W., The Astrophysical Journal, **496**: 605 (1998)

[24] Nishimichi, T., Ohmuro, H., Nakamichi, M., *et al*, Publications of the Astronomical Society of Japan, **59**: 1049 (2007)

[25] Landy, S. D., Szalay, A. S., The Astrophysical Journal, **412**: 64-71 (1993)

[26] Eisenstein, D. J., Zehavi, I., Hogg, D. W. *et al*, The Astrophysical Journal, **633**: 560-574 (2005)

[27] Komatsu, E., Smith, K. M., Dunkley, J. *et al*, Astrophysical Journal Supplement, **192**: 18 (2011)

[28] Peebles, P. J. E., Yu, J. T., The Astrophysical Journal, **162**: 815-836 (1970)

[29] Eisenstein, D. J., Hu, W., Silk, J., Szalay, A. S., The Astrophysical Journal, **494**: L1 (1998)

[30] Eisenstein, D. J., Hu, W., Tegmark, M., The Astrophysical Journal, **504**: L57 (1998)

[31] Eisenstein, D. J., arXiv:astro-ph/0301623 (2003)

[32] Seo, H. J., Eisenstein, D. J., The Astrophysical Journal, **598**: 720-740 (2003)

[33] Blake, C., Glazebrook, K., The Astrophysical Journal, **594**: 665-673 (2003)

[34] Cole, S., Percival, W. J., Peacock, J. A. *et al*, Monthly Notices of the Royal Astronomical Society, **362**: 505-534 (2005)

[35] Percival, W. J., Nichol, R. C., Eisenstein, D. J. *et al*, The Astrophysical Journal, **657**: 51-55 (2007)

[36] Tegmark, M., Eisenstein, D. J., Strauss, M. A. *et al*, Physical Review D, **74** (12): 123507 (2006)

[37] Padmanabhan, N., Xu, X., Eisenstein, D. J., *et al*, arXiv:1202.0090 (2012)

[38] Reid, B. A., Percival, W. J., Eisenstein, D. J., *et al*, Monthly Notices of the Royal Astronomical Society, **404**: 60-85 (2010)

[39] Chuang, C. H., Wang, Y., arXiv: 1209.0210 (2012)

[40] Gaztañaga, E., Cabré, A. Hui, L., Monthly Notices of the Royal Astronomical Society, **399**: 1663-1680 (2009)

[41] Drinkwater, M. J., Jurek, R. J., Blake, C., *et al*, Monthly Notices of the Royal Astronomical Society, **401**: 1429 (2010)

[42] *wigglez.swin.edu.au/site*

[43] Jones D.H., Read, M. A., Saunders, W., *et al*, Monthly Notices of the Royal Astronomical Society, **399**: 683 (2009)

[44] *www-wfau.roe.ac.uk/6dFGS*

[45] Blake, C., Kazin, E., Beutler, F., *et al*,Monthly Notices of the Royal Astronomical Society, **418**: 1707-1724 (2011)

[46] Reid, B. A., Samushia, L., White, M., *et al*, Monthly Notices of the Royal Astronomical Society, **426**: 2719-2737 (2012)

[47] Anderson, L., Aubourg, E., Bailey, S., *et al*, arXiv:1203.6594 (2012)

[48] Sánchez, A. G., Scóccola, C. G., Ross, A. J., *et al*, Monthly Notices of the Royal Astronomical Society, **425**: 415-437 (2012)

[49] Hu, W., Sugiyama, N., The Astrophysical Journal, **471**: 542 (1996)

[50] Montanari, F., Durrer, R., Physical Review D, **84**: 023522 (2011)

[51] Meiksin, A., White, M., Peacock, J. A., Monthly Notices of the Royal Astronomical Society, **304**: 851 (1999)

[52] Angulo, R., Baugh, C. M., Frenk, C. S., *et al*, Monthly Notices of the Royal Astronomical Society, **362**: L25-L29 (2005)

[53] Angulo, R., Baugh, C. M., Frenk, C. S., *et al*, Monthly Notices of the Royal Astronomical Society, **383**: 755 (2008)

[54] Springel, V., White, D. M., Jenkins, A., *et al*, Nature, **435**: 629-636 (2005)

[55] Seo, H. J., Eisenstein, D. J., The Astrophysical Journal, **633**: 575-588 (2005)

[56] Guzik, J., Bernstein, G., Smith, R. E., Monthly Notices of the Royal Astronomical Society, **375**: 1329 (2007)

[57] Smith, R. E., Scoccimarro, R., Sheth, R. K., Physical Review D, **75**: 063512 (2007)

[58] Smith, R. E., Scoccimarro, R., Sheth, R. K., Physical Review D, **77**: 043525 (2008)

[59] Xu, X., Cuesta, A. J., Padmanabhan, N., *et al*, arXiv: 1206.6732 (2012)

[60] Chuang, C. H., Wang, Y., Monthly Notices of the Royal Astronomical Society, **426**: 226-236 (2012)

[61] Faltenbacher, A., Li, C., Wang, J., The Astrophysical Journal Letters, **751**: L2 (2012)

[62] Sherwin, B. D., Zaldarriaga, M., Physical Review D, **85**: 103523 (2012)

[63] Sutherland, W., Monthly Notices of the Royal Astronomical Society, **420**: 3026 (2012)

[64] Schlegel, D., Abdalla, F., Abraham, T., *et al*, arXiv:1106.1706 (2011)

[65] Le Goff, J. M., Magneville, C., Rollinde, E., *et al*, Astronomy & Astrophysics, **534**: A135 (2011)

[66] Riess, A. G., Macri, L., Casertano, S. *et al*, The Astrophysical Journal, **699**: 539-563 (2009)

[67] Lahav, O., Suto, Y., arXiv:astro-ph/0310642 (2003)

[68] Seo, H. J., Ho, S., White, M., *et al*, arXiv:1201.2172 (2012)

[69] *http://www.astro.rug.nl/∼weygaert/tim1publication/lss2007/computerII.pdf*

[70] Blanton, M. R., Schlegel, D. J., Strauss, M. A., *et al* The Astronomical Journal, **129**: 2562 - 2578 (2005)

[71] *http://cmb.as.arizona.edu/∼eisenste/brazil/lrg_sample14.212_232.z16_47.gz*

[72] *http://cmb.as.arizona.edu/∼eisenste/brazil/random_sample14.212_232.z16_47.gz*

# Appendix A

# Taylor Expansion of the Angular Diameter Distance $\mathrm{d}_A$ Around $\Omega_K = 0$



To study the effect of curvature on the measurement of the angular diameter distance, $d_A(z)$ is expanded around $\Omega_K = 0$. In order to simplify the calculation, only the dimensionless diameter distance is considered;

$$(1+z)\frac{H_0}{c}d_A(z) = \frac{1}{\sqrt{-\Omega_K}}\sin\left(\sqrt{-\Omega_K}\int_0^z \frac{dz'}{E(z')}\right) \tag{A.1}$$

with $E(z') = (\Omega_M(1+z')^3 + \Omega_K(1+z')^2 + 1 - \Omega_M - \Omega_K)^{1/2}$. As this is valid for any redshift, $z$ is fixed to be constant. Using the substitution $x = \sqrt{-\Omega_K}$ gives the equation

$$f(x) = \frac{\sin\left(x\, g(x)\right)}{x} \tag{A.2}$$

where

$$g(x) = \int_0^z \frac{dz'}{E(x, z')} \tag{A.3}$$

Since $f(x)$ consists of a function being divided by 0 when $\Omega_K$ is set to 0, it is easier to take the expansion for

$$h(x) \equiv xf(x) = \sin\left(x\, g(x)\right) \tag{A.4}$$

The first three Taylor polynomials for $h(x)$ are

$$\frac{dh(x)}{dx} = \cos(x\, g(x))(x\, g'(x) + g(x)) \tag{A.5}$$

$$\frac{d^2h(x)}{dx^2} = -\sin(x\, g(x))(x\, g'(x) + g(x))^2 + \cos(x\, g(x))(x\, g''(x) + 2g'(x)) \tag{A.6}$$

and

$$\frac{d^3h(x)}{dx^3} = -\cos(x\,g(x))(x\,g'(x)+g(x))^3 - 3\sin(x\,g(x))(x\,g'(x)+g(x))(x\,g''(x)+2g'(x)) + \cos(x\,g(x))(x\,g'''(x)+3g''(x)) \tag{A.7}$$

where $' = d/dx$. When $x$ is set to zero, these polynomials become

$$\frac{dh(x)}{dx} = g(x) \tag{A.8}$$

$$\frac{d^2h(x)}{dx^2} = 2g'(x) \tag{A.9}$$

$$\frac{d^3h(x)}{dx^3} = 3g''(x) - g(x)^3 \tag{A.10}$$

This produces the Taylor expansion around $x = 0$

$$xf(x) = x\,g(x) + \frac{x^2}{2!}2g'(x) + \frac{x^3}{3!}(3g''(x) - g(x)^3) + \mathcal{O}(x^4) \tag{A.11}$$

Assuming that $\frac{\partial}{\partial x}\int_0^z \frac{dz'}{E(z',x)} = \int_0^z \frac{\partial}{\partial x}\frac{dz'}{E(z',x)}$, the derivatives of $g(x)$ are

$$g'(x) = -\frac{1}{2}\int_0^z \frac{2x - 2x(1+z')^2}{(\Omega_M(1+z')^3 - x^2(1+z')^2 + 1 - \Omega_M + x^2)^{3/2}}dz' \tag{A.12}$$

and

$$g''(x) = \int_0^z \frac{3}{4}\frac{(2x-2x(1+z')^2)^2}{(\Omega_M(1+z')^3 - x^2(1+z')^2 + 1 - \Omega_M + x^2)^{5/2}} - \frac{1}{2}\frac{2-2(1+z')^2}{(\Omega_M(1+z')^3 - x^2(1+z')^2 + 1 - \Omega_M + x^2)^{3/2}}dz' \tag{A.13}$$

When $x = 0$ these functions become

$$g'(x) = 0 \tag{A.14}$$

and

$$g''(x) = -\int_0^z \frac{1-(1+z')^2}{(\Omega_M(1+z')^3 + 1 - \Omega_M)^{3/2}}dz' \tag{A.15}$$

Therefore, $xf(x)$ becomes

$$xf(x) = x\,g(x) + \frac{x^3}{3!}(3g''(x) - g(x)^3) + \mathcal{O}(x^4) \tag{A.16}$$

which in turn becomes

$$f(x) = g(x) + \frac{x^2}{3!}(3g''(x) - g(x)^3) + \mathcal{O}(x^3) \tag{A.17}$$

Substituting in $g(x)$, $g''(x)$ and $x = \sqrt{-\Omega_K}$ gives

$$f(\Omega_K) = g(\Omega_K) - \frac{\Omega_K}{3!}(3g''(\Omega_K) - g(\Omega_K)^3) + \mathcal{O}(\Omega_K^2) \tag{A.18}$$

which written in full is

$$\begin{aligned} f(\Omega_K) = \int_0^z (\Omega_M(1+z')^3 + 1 - \Omega_M)^{-1/2} dz' + \frac{\Omega_K}{6}\left(\int_0^z (\Omega_M(1+z')^3 + 1 - \Omega_M)^{-1/2} dz'\right)^3 \\ + \frac{\Omega_K}{2}\int_0^z \frac{1-(1+z')^2}{(\Omega_M(1+z')^3 + 1 - \Omega_M)^{3/2}} dz' + \mathcal{O}(\Omega_K^2) \end{aligned} \tag{A.19}$$

Ignoring higher order terms and multiplying this expression by $\frac{c}{H_0(1+z)}$ gives the full expression for the Taylor expansion of $d_A(z)$ around $\Omega_K = 0$;

$$d_A(z) = \frac{c}{H_0(1+z)}\left(\int_0^z \frac{dz'}{E_{k=0}(z')} + \frac{\Omega_K}{6}\left(\int_0^z \frac{dz'}{E_{k=0}(z')}\right)^3 + \frac{\Omega_K}{2}\int_0^z \frac{1-(1+z')^2}{E_{k=0}(z')^3} dz'\right) \tag{A.20}$$

where

$$E_{k=0}(z) = \left(\Omega_M(1+z)^3 + 1 - \Omega_M\right)^{1/2} \tag{A.21}$$

is the Hubble parameter for $\Omega_K = 0$.

# Appendix B

# The Python Script for the 2-Point Correlation Function



```
from math import *
from numpy import *
from scipy import integrate
from scipy.interpolate import InterpolatedUnivariateSpline
fg = open("lrg", "r")
fd = open("random", "r")
sd = open("bao", "w")
# Values for the cosmic parameters
c = 3.0*10**5
Om = 0.3
H0 = 72.0
Ol = 0.7
rty = 2.0
# Formula for radial diameter distance
func = lambda z: 1.0/sqrt(Om*(1.0 + z)**3 +0.7)
listyy = []
listss = []
ss = 0.01
# Integrating the radial distance and forming the angular
diameter distance with a spline of the radial distance
while ss <= rty:
      y, err = integrate.quad(func, 0.0, ss)
```

```
      listss.append(ss)
      listyy.append(y)
      ss = ss + 0.01
Hz = InterpolatedUnivariateSpline(listss, listyy)
def angdist(zz):
      value = c*(1.0 + zz)/H0 * Hz(zz)
      return(value)

listxD = []
listyD = []
listzD = []
weightD = []
listxR = []
listyR = []
listzR = []
weightR = []
a = 1
b = 2
n = 0
k = 0
for line in fg:
  red = float(line.split()[0])
  angle = float(line.split()[1])
  dec = float(line.split()[2])
  weight = float(line.split()[3])
  dist = angdist(red)
  # Converting declination into polar angle
  dd = (pi/2.0) - dec
  # Converting into spherical coordinates
  xx = dist*cos(angle)*sin(dd)
  yy = dist*sin(angle)*sin(dd)
  zz = dist*cos(dd)
  listxD.append(xx)
  listyD.append(yy)
  listzD.append(zz)
```

```
  weightD.append(weight)
  n = n + 1
# As above but for the random catalogue
for line in fd:
  red = float(line.split()[0])
  angle = float(line.split()[1])
  dec = float(line.split()[2])
  weight = float(line.split()[3])
  dist = angdist(red)
  dd = (pi/2.0) - dec
  xx = dist*cos(angle)*sin(dd)
  yy = dist*sin(angle)*sin(dd)
  zz = dist*cos(dd)
  listxR.append(xx)
  listyR.append(yy)
  listzR.append(zz)
  weightR.append(weight)
  k = k + 1

fuzzy = 0
compare = 100000
bins = 201
# This is the size of the bins
size = 1.0
counter = 0
listD = bins*[0]
listR = bins*[0]
listDR = bins*[0]
# To reduce computation time, instead of checking if distances are less
than 200 Mpc, instead check off against 200^2. This prevents the code
from unnecessarily doing a square root for every calculation.
comp = 40000.0
m = 0
while m < n:
  x0 = listxD[m]
```

```
y0 = listyD[m]
z0 = listzD[m]
w = weightD[m]
# Setting the parameter space around the origin galaxy
u = x0 + 200.0
i = x0 - 200.0
o = y0 + 200.0
p = y0 - 200.0
r = z0 + 200.0
t = z0 - 200.0
listxt = []
listyt = []
listzt = []
wwt = []
oo = 0
for j in range(m + 1, n):
  x1 = listxD[j]
  y1 = listyD[j]
  z1 = listzD[j]
  ww1 = weightD[j]
  #Checking to see which galaxies are within the volume demarcated around
  the origin galaxy
  if i < x1 < u and p < y1 < o and t < z1 < r:
    listxt.append(x1)
    listyt.append(y1)
    listzt.append(z1)
    wwt.append(ww1)
    oo = oo + 1
for e in range(0, oo):
  x2 = listxt[e]
  y2 = listyt[e]
  z2 = listzt[e]
  ww2 = wwt[e]
  # Calculating the distance from the x, y, z coordinates
  dd = (x0 - x2)**2 + (y0 - y2)**2 + (z0 - z2)**2
```

```
    if dd <= comp:
      # Checking to see which bin the distance is to be assigned to
      ds = int(sqrt(dd)/size)
      io = ww2 * w
      listD[ds] = listD[ds] + io
      counter = counter + 1
      fuzzy = fuzzy + 1
      if fuzzy == compare:
        print fuzzy
        compare = compare + 100000
  m = m + 1
# As above but now for the DR correlation
v = 0
while v < n:
  x0 = listxD[v]
  y0 = listyD[v]
  z0 = listzD[v]
  w = weightD[v]
  u = x0 + 200.0
  i = x0 - 200.0
  o = y0 + 200.0
  p = y0 - 200.0
  r = z0 + 200.0
  t = z0 - 200.0
  listxt = []
  listyt = []
  listzt = []
  wwt = []
  oo = 0
  for j in range(0, k):
    x1 = listxR[j]
    y1 = listyR[j]
    z1 = listzR[j]
    ww1 = weightR[j]
    if i < x1 < u and p < y1 < o and t < z1 < r:
```

```
      listxt.append(x1)
      listyt.append(y1)
      listzt.append(z1)
      wwt.append(ww1)
      oo = oo + 1
  for e in range(0, oo):
    x2 = listxt[e]
    y2 = listyt[e]
    z2 = listzt[e]
    ww2 = wwt[e]
    dd = (x0 - x2)**2 + (y0 - y2)**2 + (z0 - z2)**2
    if dd <= comp:
      ds = int(sqrt(dd)/size)
      io = ww2 * w
      listDR[ds] = listDR[ds] + io
      counter = counter + 1
      fuzzy = fuzzy + 1
      if fuzzy == compare:
        print fuzzy
        compare = compare + 100000
  v = v + 1
# As above for the RR correlation
q = 0
while q < k:
  x0 = listxR[q]
  y0 = listyR[q]
  z0 = listzR[q]
  w = weightR[q]
  u = x0 + 200.0
  i = x0 - 200.0
  o = y0 + 200.0
  p = y0 - 200.0
  r = z0 + 200.0
  t = z0 - 200.0
  listxt = []
```

```
  listyt = []
  listzt = []
  wwt = []
  oo = 0
  for j in range(q + 1, k):
    x1 = listxR[j]
    y1 = listyR[j]
    z1 = listzR[j]
    ww1 = weightR[j]
    if i < x1 < u and p < y1 < o and t < z1 < r:
      listxt.append(x1)
      listyt.append(y1)
      listzt.append(z1)
      wwt.append(ww1)
      oo = oo + 1
  for e in range(0, oo):
    x2 = listxt[e]
    y2 = listyt[e]
    z2 = listzt[e]
    ww2 = wwt[e]
    dd = (x0 - x2)**2 + (y0 - y2)**2 + (z0 - z2)**2
    if dd <= comp:
      ds = int(sqrt(dd)/size)
      io = ww2 * w
      listR[ds] = listR[ds] + io
      counter = counter + 1
      fuzzy = fuzzy + 1
      if fuzzy == compare:
        print fuzzy
        compare = compare + 100000
  q = q + 1
# Writing the DD, DR and RR bins to file where they will then be used to
calculate the 2-point correlation function
for l in range(0, bins):
    xl = listD[l]
```

```
    fr = listDR[l]
    op = listR[l]
    er = l * size
    sd.write("%f %f %f %f\n" % (er, xl, fr, op))

print counter
fg.close()
fd.close()
sd.close()
```